Finite Element Analysis for the Damage Detection of Light Pole Structures

BY

Qixiang Tang
Bachelor of Science in Civil and Environmental Engineering
Shenzhen University, Shenzhen, China

SUBMITTED IN PARTIAL FULFILLMENT OF THE REQUIREMENTS
FOR THE DEGREE OF MASTER OF SCIENCE
DEPARTMENT OF CIVIL AND ENVIRONMENTAL ENGINEERING
UNIVERSITY OF MASSACHUSETTS LOWELL

Signature of the Author .....
Department of Civil and Environmental Engineering
July, 2014

Signature of Thesis Supervisor .....
Professor Tzuyang Yu
Department of Civil and Environmental Engineering

Committee Member Signature .....
Professor Peter Avitabile
Department of Mechanical Engineering

Committee Member Signature .....
Professor Murat Inalpolat
Department of Mechanical Engineering

Committee Member Signature .....
Professor Susan Faraji
Department of Civil and Environmental Engineering

Finite Element Analysis for the Damage Detection of Light Pole Structures

BY

Qixiang Tang
Bachelor of Science in Civil and Environmental Engineering
Shenzhen University, Shenzhen, China

ABSTRACT OF A THESIS SUBMITTED TO THE FACULTY OF THE
DEPARTMENT OF CIVIL AND ENVIRONMENTAL ENGINEERING
IN PARTIAL FULFILLMENT OF THE REQUIREMENTS
FOR THE DEGREE OF
MASTER OF SCIENCE
UNIVERSITY OF MASSACHUSETTS LOWELL
2014

Thesis Supervisor: Tzuyang Yu
Title: Professor

Abstract

Light pole structures are commonly installed in everywhere of human society. Aging of light poles is unstoppable and inevitable, and eventually cause failures of light poles. Potential failures of light poles are detrimental to public safety since they bring risks to nearby residents and damage adjacent structures. Effective damage detection methods for light poles are hence required.

Any change in structural properties (e.g., mass, stiffness) can lead to differences in the dynamic response of structures, such as modal frequencies and mode shapes. Inversely, changes in dynamical responses can be used as indicators for damage detection.

In this study, a straight steel tubing light pole was used as an example. The relationships among damages and dynamic responses (modal frequencies and mode shapes) were determined by observing the differences in dynamic responses between intact and artificially damaged finite element models (developed with ABAQUS®) of the example light pole. Inversely, damage detection methods were developed by using determined relationships. Proposed methodology was to use sensitive modes which were determined for three common damage locations, to localize damage. Then, use linear regression equations to qualify damage level and size. A damage detection methodology using mode shapes are also proposed in this study.

Acknowledgments

Foremost, I would like to express my sincere gratitude to my advisor Professor Tzuyang Yu for his invaluable help and support from the first day of this project as well as his technical guidance, endless forbearance, and constant encouragement. Besides my advisor, I would like to thank the rest of my thesis committee: Prof. Peter Avitabile, Prof. Murat Inalpolat and Prof.Susan Faraji for their insightful comments.

My sincere thanks also goes to my friend and my fellow labmates: Jones Owusu Twumasi and Ross Gladstone, for their kind helps and suggestions.

At last but not least, I would like to thank my family for their support throughout my life.

Contents

List of Figures

List of Tables

List of Symbols

ω	Intact model's modal frequency
$\Delta\omega$	Modal frequency difference
Δf_i^j	Modal frequency difference in ith mode, and the damage locates at L_j
i	Vibration mode
L_j	Damage location, j various from 1 to 3
A	Cross-sectional area of a FE pole model
α	Ratio of total cross-sectional area that is damaged
αA	Cross-sectional area of damaged region in a FE pole model
E	Young's modulus of material
β	Reduction rate of Young's modulus in damage region
$\hat{m}$	Generalized mass
$\hat{k}$	Generalized stiffness
$\Psi(x)$	Shape function
$m(x)$	Mass function
$I(x)$	Moment of inertia function

x	position of an arbitrary point in axis along the height of pole
Φ	Displacement of mode shape
Φ''	Curvatures of mode shape
$\Delta\Phi$	Changes in displacement of mode shape
$\Delta\Phi''$	Changes in curvature of mode shape

Chapter 1

Introduction

1.1 Problem statement

Aging of structure reduces structural integrity and is inevitable and unstoppable. Light poles, like other man-made structures, are susceptible to failures due to aging. Light pole structures have been widely installed in human society, potential failures of light poles are crucial to public safety since they bring risks to nearby residents and damage adjacent structures (e.g. residential houses, electricity boxes.)

Common causes of light poles failure seen in recent years have the following characteristics [2]:

- Toe cracks in the pole structure shaft wall above the base plate weld that propagate along the weld over time causing the pole to collapse.

- Thin base plates (under-designed) allowing for excessive movement resulting in fatigue at the base plate/pole wall welded connection.

- Anchor bolt failure which cause separation of pole structure and foundation.

The corresponding light pole components that aforementioned characteristics (of light pole's failure) appear in, are shown in Fig. 1-1 [1]:

Under long term loading effects in combination with any of the above characteristics,

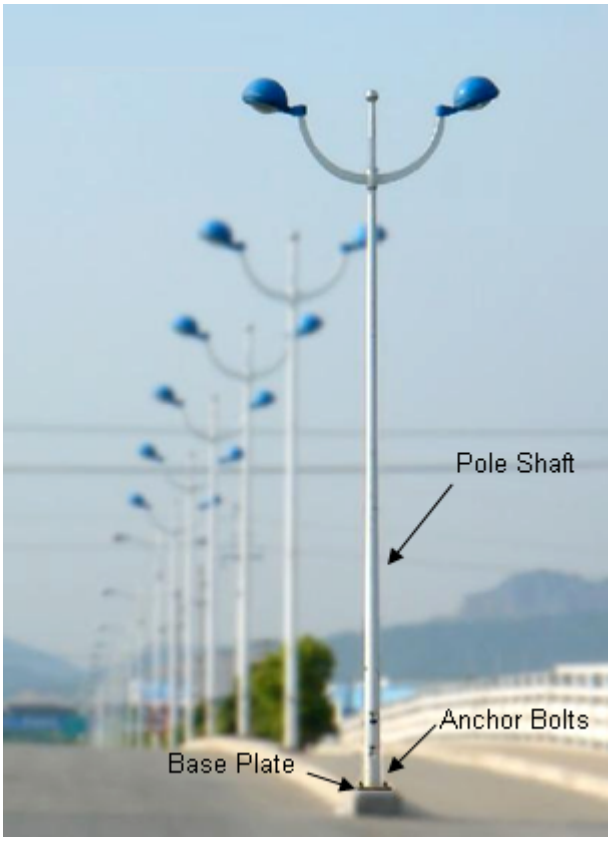

Figure 1-1: Components that may cause light pole's failure [1]

a light pole is highly susceptible to fatigue failure. In December 2009, a 200-pound corroded light pole fell across the southeast expressway in Massachusetts [3]. Three

other damaged poles were removed. The incident shocked civil engineers and they began a daunting task to closely examining more than 4,000 poles in the common wealth of Massachusetts, which had never been done before. In October 2012, the Commonwealth of Massachusetts tried to come up with millions of dollars to fix this growing problem of light poles before more injuries occur. [3]

However, the precondition of all maintenance procedures such as repair and replacement, is knowing the conditions of light poles(e.g., is a light pole damaged or not? where is the damage?). The need for reliable and efficient damage detection techniques is raised for solving these problems.

Damage detection techniques using changes in the dynamic modal responses of a structure (e.g. modal frequency and mode shape) have been a hot research topic in damage detection area since last century. Structural dynamic responses such as modal frequencies are independent to loading conditions and are directly affected by changes in structural physical properties (e.g., stiffness and mass), therefore, the corresponding damage detection techniques are consider as appropriate methods for light poles.

Even though those methods are effective for damage detection, they are time consuming for research experiment. Therefore, in this research, numerical approach were conducted instead of testing. Using numerical simulation, sufficient amount of data can be gathered without being constrained by limited time and resources required in conducting experiments for a thorough investigation on the research problem.

1.2 Research objective

The primary contribution this study is to develop a damage detection methodology for light poles structures, using finite element simulations.

1.3 Thesis approach

This study proposes a methodology to localize and quantify common damages in light poles by investigating the different dynamic behaviors in free vibration. Two dynamic characteristics-modal frequencies and mode shapes were chosen as the parameters for condition assessments. The parameters of interest were generated by finite element (FE) modeling. All FE models of light poles are created with ABAQUS®, a popular commercial FE package.

A steel tapered light pole from manufacturer ELEKTROMONTAÅ RZESZW SA was chosen as the example for intact light pole structures. A FE model of the steel tapered light pole was generated as the intact model. It was validated by comparing the modal frequency of the first mode with theoretical calculation. Post-damage FE models were produced by introducing artificial damages to the intact FE model. With the advantages of FE modeling, many damage cases can be considered. Artificial damages can occur at different locations with different levels. The research approach is to uncover the influences of damages by finding out the pattern in modal frequencies and mode shapes due to the presence of damage. However, in each damaged model, only one artificial damage was introduced.

In this research, research tasks include

- Develop a FE model of an intact light pole.
- Validate the FE model using the Rayleigh's Method.
- Develop damaged light pole models by inflicting artificial damages to the intact model.
- Determine relationships between damage's locations and changes in modal frequencies/mode shapes.
- Determine relationships between damage's severities and changes in modal frequencies/mode shapes.
- Propose a damage detection methodology to localize and quantify a damage in a light pole.

Fig. 1-2provides the research roadmap in this thesis.

1.4 Organization of the Thesis

The organization of this thesis is in the following.

Chapter 2 reports the literatures related to the research topic. The literature review is divided into three categories. First, survey the failure mechanisms of light poles. Secondly, investigate the FE techniques for simulating light pole structures under free vibration. In addition, review techniques for validating FE models and improving the

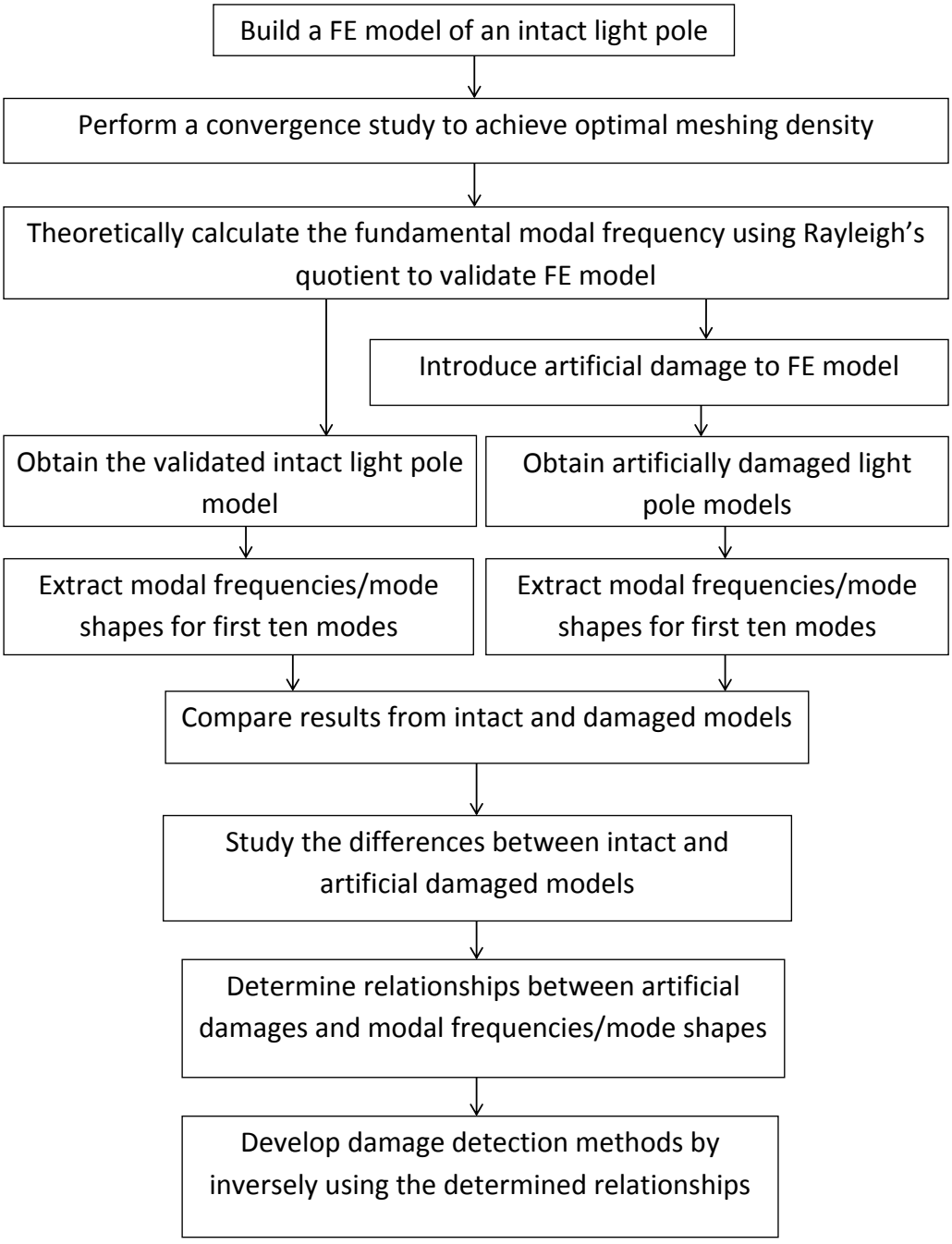

Figure 1-2: Research roadmap

accuracy of FE models. Thirdly, survey existing damage detection methods using dynamic responses.

Chapter 3 describes research strategies and approaches. Selection of parameters is discussed. FE modeling techniques of light poles were also discussed. Followed by details of intact and damaged model including geometry, material properties and meshing techniques. Three attributes of artificial damages in light poles are defined. At last, a convergence study and theoretical calculation of the intact model were conducted to validate FE models .

Chapter 4 presents FE simulation results. Modal frequencies and mode shapes of the FE models are reported. Results of different damage scenarios are analyzed and discussed. A methodology of damage detection for light poles are proposed at last.

Chapter 5 summarizes research findings, contributions and suggests future work for this research.

Chapter 2

Literature Review

2.1 Introduction

The literature review is divided into three parts. Firstly, a survey of failure mechanisms of light poles is provided. Secondly, investigation of FE modeling techniques using ABAQUS® for simulating light poles is conducted. Thirdly, structural damage detection methodologies using dynamic characteristics (modal frequencies and mode shapes) are reviewed.

2.2 Mechanisms of light poles' failure:

For decades, tubular steel poles have been utilized as a support structure in utility, sports lighting, and transportation industries. Failures of pole structures in different states had been reported during past decades [4]. Considering the danger and risk of the poles' collapse, as well as the robustness and safety of existing infrastructure inventories, a

number of investigations have been conducted to study the failure mechanisms of pole structures. Possible causes of poles' failure and location of common defects have been reported in the following review.

Garlich and Thorkildsen (2005) [5] reported necessary wind loads which can fail pole structures. Poles must be strong enough to withstand not only the maximum expected loads, but also long term fatigue effects of wind load. Four wind-loading phenomena can contribute to support (pole) structures' vibration and fatigue: i) natural wind gusts, ii) truck-induced gusts, iii) vortex shedding and iv) galloping. Each type of support structures (e.g., signal, sign, or luminaires) is vulnerable to either two or three of the four wind loads depended on its stiffness and shape. For luminaires structures(e.g.light poles), natural wind gusts and vortex shedding are the primary load-effects.

Natural wind gusts introduce a horizontal fluctuating force which result in horizontal motion of the mast arm. Consequently, fatigue cracking is caused and then developed over a period of several years at least. In light poles, the connection of the arm supporting the lights to the pole top has high possibilities to crack. Natural wind gust loading also causes cracks at the base of the pole, at the weld joining the pole to the base plate, at the top of the stiffeners, at hand holes, or at the anchor rods. Vortex shedding occurs on alternate sides that happens to symmetric member. It results in resonant oscillation of poles and their collapse. Among all types of utility poles, only luminaries support structures may occasionally exhibit excessive vibration by vortex shedding. If vortex shedding persisted long enough, fatigue cracking would be caused within a short pe-

riod. For example, one night of windstorm is longer enough for fatigue cracks of light pole initiate and propagate to failure. In light poles, cracks (caused by vortex shedding) are usually observed at the base of the pole or at the weld joining the pole to the base plate or transformer base.

It was also mentioned that cracks are caused by fatigue, rather than overloading the structures. Fatigue failure of a support (pole) structure basically occurs when the stress ranges resulting from external excitations exceed the fatigue thresholds at critical details, such as aforementioned crack locations. Usually, these fatigue failures are an indication that the structure is designed inadequately for current load condition and is experiencing excessively large stress ranges and other similar structures will soon be facing similar cracking problems. Therefore, if a fatigue failure has occurred in a structure, other similar structures in similar environment are suspicious to fatigue failure and should be intensively inspected immediately.

In their report, some geometry details were also mentioned. According to NCHRP Report 412 [6], the base plate thickness should be greater than anchor rod diameter, in order to provide even distribution of the load and to minimize prying forces. In addition, the distance from the center of the anchor rod hole to the edge of the base plate should be greater than two times the nominal diameter of the anchor rod.

Caracoglia and Jones (2004) [7] studied two different cases of light poles' failures. In the first case (Western Illinois pole failures) the poles failed due to the excessive amplitude of oscillation induced in a wind storm. About 140 poles collapsed in this case. In the second case (I-80) Bridge light pole lamp failures) light bulbs failed also

due to oscillation. In the first case, two mechanisms of failure were defined: maximum capacity of the material,and fatigue due to long-term cyclic loads. In their report, three failure sources of excitation were identified: i) buffeting under turbulent winds, ii) vortex-induced vibration (at lock-in) and iii) galloping due to aerodynamic modifications (frozen accumulation on the surface of the poles). The combinations of one or more of the above were also possible. They also conducted analytical investigation. The result was confirmed by comparing with FE simulation. It was suggested that the wind characteristics necessary to exceed the load capacity of light poles were not consistent with the meteorological report for the Western Illinois pole failure incident. This means first failure mechanism was unlikely to be responsible for these failures. Furthermore, the circular section was immune from galloping until the presence of frozen precipitation (formed by rain or snow close to freezing temperature during the snowstorm) on the surface. This phenomenon can be associated with large-amplitude vibrations, at frequencies lower than the one of vortex shedding, which could be a more plausible explanation. In the second case, a FE simulation was developed in order to gather the information of natural frequency and mode shapes of light poles. Experiments were performed to confirm the results of numerical simulation. All results suggest that the second in-plane mode shape, at a frequency around 4 Hz, is the cause of high accelerations associated with the failures of lamps.

Conner *et. al.* (2005) [4] reported a long-term, in-depth field experimental study on the dynamic behavior of fatigued high-mast lighting structures. The study was prompted by a collapse of a high-mast lighting tower along I-29 near Sioux City on

November 12, 2003. A statewide inspection was conducted of all 233 high-mast lighting towers after the incident. Investigations indicated that fatigue cracking is the cause of most of pole failures, either at the base plate-to-column weld, or at the handhole detail, or of anchor rods. A FE study was conducted for the as-built pole structures focusing on the impacts of base plate thickness and on the distribution of stresses in the tube wall at the weld. The results demonstrated: 1) the base plate in the failed poles was not thick enough to prevent substantial out-of-plane local bending stresses to develop in the tube wall. 2) Loose nuts significantly increase the axial forces in other anchor rods and the bending stresses stress at the base plate-to-tube welded connection.

A controlled load and long-term remote monitoring program was also applied to obtain the experimental data of dynamic characteristics. Dynamic properties of the towers were determined from a 'pluck' test. The vibration modes of interest in this study are the first four modes. The pluck test results were consistent with measured data, which confirmed the reliability of the pluck test. Based on the results of this study and the observations of other failures, the bottom sections of high mast towers should be visually inspected at the base weld and at handhole on a regular basis. Anchor rods also need to be inspected since the risk of their fatigue failure is critical.

In review of reported research (Garlich and Thorkildsen (2005), Caracoglia and Jones (2004); Conner *et. al.* (2005)), a brief conclusion can be made: 1) natural wind gust and vortex shedding introduce fatigue to pole structure; 2) cracks are caused by fatigue, rather than overload; 3) if one pole failed due to fatigue, other similar poles are suspicious; 4) three common damage (crack) locations in light poles were suggested as:

i) pole-to-transverse plate connection, ii) handhole detail and iii) anchor bolts. Anchor bolt's failure is not considered in this thesis.

2.3 FE modeling of light poles

Yan *et. al.* (2006) [8] proposed an improved modeling method based on modifying local (element) stiffness matrix at structural damage position, in order to overcome the difficulties of meshing small structural damages in FE models. There are two problems when directly meshing small structural damage in FE modeling: i) the demand of excessive griding number and ii) unavoidable errors from differently meshing for the same damaged structure. The proposed method included the determination of modification coefficients element stiffness matrix and the verification of coherence between frequency-response functions for two different models. Since the improved method can decrease the number of required elements for modeling small structural damage, the efficiency of dynamics analysis for damaged structures increased.

Damage in a structure always reduces structural stiffness, so that these variations can be expressed using changes in material's property (Young's modulus) of the local structure. Structural damages can be simulated in FE models using the modified material Young's modulus in local damage position, and it is unnecessary to depict the geometry of small damage exactly. Hence, avoiding two aforementioned problems caused by direct meshing structures in modeling damaged structures becomes possible.

The method herein involves two steps: 1) meshing a intact structure, 2) for those elements in position of structural damage, modify their element stiffness matrices to sim-

ulate structural damage. In order to obtain the modification that describe the damage best, optimal equivalent principle is used. For instance, when establishing a dynamics model of a damaged structure, different values of modification are tested until achieving the lowest statistical error of modal frequencies between two kinds of models with different damage meshing techniques.

A discussion about the "detectable size" of structural damage and their corresponding detection method was also presented. Generally, the size of structural damage can be approximately divided into three levels: (1) micro-damage– damage size is smaller than 0.1% of structural size(volume). Vibration-based detection method is not efficient for this type of damage. It could be detected by instruments with high precision, such as Computerized tomography (CT) scan, ultrasonic wave, etc. However, structural micro-damage may produce very little influence on structural safety life. (2) small-damage– damage size is about 1% of structural volume. Structural small damages have a large chance to develop into macro-damage, therefore, it possesses the potential harm to in-service structures. Hence, it is necessary to inspect for structural small-damage during their usage.; (3) macro-damage– damage size is greater than 10% of structural size. The structure with macro-damage often have been destroyed. Damages usually can be found using naked eye or other simple method.

In summary, based on the analysis for existing problems in modeling small structural damage using current commercial structural analysis software, an improved modeling method was proposed. In this method small structural damage is expressed using variations of stiffness matrix of several elements, hence superfluous FE griding was avoided. The new method was more efficient for obtaining structural dynamic response, which

will be used for structural damage detection.

Le *et. al.* (2008) [9] studied the relationships between modal frequency of long tapered hollow poles and their geometrical variables(pole length, top and bottom diameters of pole, bolt diameter, etc) based on three-dimensional FE model analyses by taking into account the couplings between material, contact and geometric nonlinearities. The FEM results are verified by the experimental data obtained from a 60 ft pole. A sensitivity study was also conducted to identify the effect of different geometric parameters on modal frequencies of the pole. Three empirical formulae between the geometric variables and the first, second and third mode modal frequencies were obtained. Using finite element modeling, three empirical formulas were developed. The FEM results were verified by experimental data. The geometric parameters considered herein are the pole's: length, top and bottom diameters; bolt diameter; thickness; and end-plate thickness. Various types of elements were tested to obtain the optimum finite element mesh. The 8-node solid element was selected for pole structure because of its accuracy and simplicity. One half of a typical pole is modeled since the structure is symmetric. Meanwhile, another type of element - tetrahedron element was applied to the bolts. Dynamic analyses of poles were performed using ABAQUS®. Modal frequencies of the poles and corresponding mode shapes were obtained by using Lanczo's Eigenvalue Extraction Method [10]. Initial stress and load stiffness effects due to preloads and initial conditions were considered in FE analysis; Self-weight was also taken into account. The optimum mesh density was determined by conducting a convergence study performed for a typical pole case and with different mesh densities. The interaction

between contact surfaces of the bolt head, the shank, and the nut with the end-plate and bolt holes were simulated by surface-to-surface [10] contact algorithm. The converged solution from FE model dynamical analysis was verified by exact solutions presented by Jacobsen and Ayre [21] for a typical pole with fixed support for model verification. Experimental data of a 60 ft height pole was obtained from field tests for further verifying the numerical results. Parametric study was conducted on verified FE model in order to identify the impact of varying geometric parameters the pole. It is found that increasing the pole length and/or pole thickness at the top decreases of first three modal frequencies. In addition, increasing the diameter of the pole at bottom and/or the diameter of bolt circle,the modal frequencies of the first three modes increase as results. The cause of these changes were caused by the varieties in structural stiffness introduced by varying the geometric parameters. The modal frequencies become larger while structural stiffness becomes stiffer and vice versa.It was also claimed that the changes in these geometric parameters are irrelevant to each other. Three empirical formulas were developed to indicate the relationships between the geometric parameters and the first three modal frequencies for the long tapered hollow steel poles, using the results from the parametric study.

In summary, FE models can simulate the dynamical behavior of steel poles. FE model results shows good agreement with experimental result. The literature study also shows that structural damages in light poles can be expressed as reduction in local materials' properties (i.e. Young's modulus) in FE models. Modal frequencies can be effected by the changes in structural stiffness.

2.4 Damage detection techniques

Generally, structural damage detection can be divided into five levels: (1) identification of damage existence in a structure, (2) localization of damage, (3) identification of the damage type, (4) quantification of damage severity, and (5) prediction of the remaining service life of the structure [11]. The basic problems for structural damage detection are how to ascertain presence, location and severity of structural damage using measured parameters.

Yan *et. al.* (2007) [12] presented a general review and summary of vibration-based structural damage detection techniques using dynamic response.

In their review, structural damage detection techniques can be classified into two groups: local-damage detection [13] and global-damage detection. Local-damage detection techniques, such as computed tomography (CT) scanning and ultrasonic, etc., is mainly used to determine existence and location of local damage in structures with only data obtained from damaged structure. However, in large and complicated structures, using local damage detection methods is very difficult. In order to detect damage in such conditions, global vibration-based structural damage detection has been proposed [14, 15]. Structures' global dynamical characteristics(stiffness, mass and damping)are changed by the presence of damage, which cause changes in frequency-response function and modal parameters of structures. Therefore, the change of modal parameters can be taken as the index of damage presence[16, 17]. Vibration-based structural damage detection have became a popular research topic because it can solve this particular prob-

lem. Methods of vibration-based damage detection can be categorized into traditional- and modern-type. The traditional structural damage detection methods are mainly based on the free vibration characteristics of the structures, such as modal frequencies or mode shapes. Since loss in stiffness and material strength in damaged region, modal frequencies and mode shapes will be changed accordingly. Assessment of structural damage is equivalent to determining and quantifying structural characteristics of the damaged region, by comparing to intact region. However, there are three disadvantages: (i) it is time-consuming and expensive to conduct experiments, (ii) the traditional methods are more dependent on the properties of individual structures. It is difficult to establish a universal methodology for all structures, and (iii) the traditional methods are usually not sensitive to initial damage in structures. The parameters that can be used in traditional methods include: modal frequency [18, 19], vibration mode shape [20, 21], structural flexibility or stiffness [22, 23], transfer function(frequency-response function) [24, 25] and statistic information [26, 27, 28] and power flow [29, 30].

The modern structure damage detection methods called intelligent damage diagnosis. It is based on on-line measured structural vibration responses to detect damage, mainly using modern signal-processing techniques and artificial intelligence. Modern methods are universal for different structures, and are independent on structural properties, comparing with traditional methods. The modern methods do not require many experiments. Only few points in the structure under investigation are needed for inspection. Thus, structural shutdown or production halt is avoided. Using the modern methods, smaller/initial structural damages can be detected by extracting better structural characteristics from structural dynamic response signals. The representative modern methods

include: wavelet analysis [31, 32, 33, 34], Genetic algorithm (GA) [35, 36, 37] and Artificial Neural Network (NN) [38, 39, 40]. However, there are still several problems in modern methods, such as: (1) these methods have to rely on the environmental excitation; (2) the measured signals are possibly affected by background noise.

2.4.1 Modal frequency-based damage detection methods

Lee and Chung (2000) [41] proposed a simple nondestructive evaluation procedure for identifying the location and size of a crack in a one-dimensional cantilever-beam, using lowest four modal frequencies. The first step is to find the lowest four modal frequencies of the cracked structure by FE method. The FE model used in this paper was made by modified Reddy's general FEM1D [27]. The modified FE model was validated by comparing lowest three modal frequencies to the experimental results and to Gudmundson's theory results [42]. Then, arrange the mode numbers based on eigenfrequency shifts in decreasing order by Armon's Rank-ordering method [43]. The eigenfrequency shift is defined as:

$$\frac{\Delta\omega}{\omega} = \frac{uncracked\ frequency - cracked\ frequency}{uncracked\ frequency} * 100\% \tag{2.1}$$

The approximate crack location is estimated by the ranked mode numbers. For example, the rank ordering as 1234 represents a crack locate near 0 to 0.11 of length of the beam. Inversely, applying the result of the crack position range, the appropriate FE model can be adopted and the crack size is hence determined.

Finally, the actual crack location can be identified by Gudmundson's equation using

the determined crack size and the aforementioned lowest four modal frequencies. In their conclusion, although the error (fractional difference between FE results and experimental results) of this method in the example of the fourth mode was large as 25%, it still can be claimed as an easier method for detecting a crack in a one dimensional cantilever beam. However, there are some disadvantages of this method: 1) this method was developed based on one dimensional structures, its applicability to real structure is in question; 2) only single crack (damage) was considered in this study, proposed method needs to be adjusted for multiple damage scenarios; 3) instead of only lowest four modal frequencies considered in this method, more modal frequencies might be used for further development.

Kim and Stubbs (2003) [44] presented a nondestructive method to locate and quantify a crack in structures with only few modal frequencies. The first part of their paper presented a theory of crack detection. The information about damage location and size of crack were directly obtained by using changes in modal frequencies of the structure. A crack estimation model, relating fractional changes in modal energy to changes in modal frequencies, was hence formulated. A demonstration of the feasibility and practicality of proposed method was made by applying the approach to damaged beams for which four modal frequencies were measured. By plotting damage indicator DI_j (Kim and Stubbs 2003[44]) against normalized length of the beam, a peak value can be found at the location of the crack. Their result showed that the crack can be confidently localized and qualified with relatively small errors. As they concluded, it is possible to determine crack location and size of a crack in a beam-type structure.

Owolabi *et. al.* (2003) [45] reported detailed experimental investigations of the effects of damages on lowest three modes of vibrating beams. The dynamic responses (modal frequencies and mode shapes) of the beams showed very high sensitivities to the crack location and crack depth. A simple method for predicting the location(s) and depth(s) of the crack(s) based on changes in the modal frequencies and amplitudes of the frequency-response-functions (FRF) of the beam was proposed and discussed in their report.

For a beam with a single crack, the following steps are required for damage assessment: (1) measurements of the lowest three modal frequencies; (2) normalization of the measured frequencies; (3) plotting of contour lines from different modes on the same axes; and (4) locating intersection point(s) of the different contour lines. The intersection point(s), common to all the three modes, indicate(s) the crack location(s), and crack depth(s). If there were more parameters that influence the response, more modes are required to identify the unknown crack depth and crack location. Even though the method proposed here is simple and feasible, there are some disadvantages. First of all, in order to achieve sufficient accuracy, this method requires massive data of intact and damaged structures. Secondly, if those information is not accurate enough, the intersection points (used to identify crack locations and depths) are difficult to find in contours plots.

2.4.2 Mode shape-based damage detection methods

Abdo and Hori (2002) [46] presented a numerical study on the relationship between damage characteristics and the changes in dynamic properties. They reported that the rotation of mode shape is a sensitive damage indicator. (The rotation of mode shape is computed by taking derivatives of mode shape displacements.) The numerical results clarify that the rotation of mode shape has the characteristic of localization at the damaged region while the mode shape displacement sometime has not. Also,the rotations of modes are robust in locating multiple damage locations with different sizes in a structure. Furthermore, using the changes in the rotation of mode shape does not need very accurate measurements to detect and locate damage,comparing to modal frequencies. An example of damage detection of a plate were given for illustration. The first five modal frequencies of the plate for different cases of damage scenarios shows that there are discernible changes in the modal frequencies between the intact and damaged plate, however, this does not give an indication of the location of damage. Unlikely, on the plots of the absolute differences of the rotation of mode shapes between the intact and damaged cantilever plate, it can be easily seen that that the rotations of mode shapes are localized at the damaged region for all cases of damage.

The results of the steel plate model demonstrate the possibility of using the changes in the rotation of mode shape as a diagnostic parameter in damage detection. It was suggest that changes in the derivative (rotation or slope) of the mode shapes are more sensitive than in displacement. Also, the rotation of mode is localized in the region of damage for initiation or extension of damage. The advantages of using changes in

the above index is that it does not need higher modes of the structure. In addition, this method has the ability to pinpoint a small amount of damage, which may represent initial damage. Finally, the rotation of mode shape is likely to be recorded on-site. However, taking derivative of mode shape displacements amplifies noise in practice, which might affect accuracy of this indicator.

Kim *et. al.* (2011) [47] presented a methodology to nondestructively locate and estimate the size of damage in structures. In this methodology, first of all, a frequency-based damage detection (FBDD) method was proposed. This method includes a damage-localization algorithm that locates damage by using the changes in modal frequencies, and a damage-sizing algorithm that estimates crack size from modal frequency shift. Next, a mode-shape-based damage detection (MBDD) method was discussed. A damage index algorithm that localizes and qualifies damage based on changes in modal strain energy was formulated. The FBDD method and the MBDD method were evaluated for several damage scenarios by applying them to numerically simulated prestressed concrete beams with only two sets of modal parameters were available. For the verification, the test results were compared to modal frequencies and mode shapes of the first two vibration modes of which generated from FE models. The damage in the test structure could be located by FBDD approach with a relatively small localization error. In a 3.6 m beam span, the predicted locations fell within 1 cm of the correct locations while the cracks is near the midspan; and within 13.7 cm while the cracks near the left quarter-span of the correct locations in a 3.6 meter beam span. By applying the MBDD approach, damages in test structure can also be located accurately. In a 3.6

m beam span, the predicted locations were identical to the inflicted locations when the cracks are near the mid-span and within 6.25 cm from the correct locations when the cracks are near the left quarter-span. However, it was also observed that the accuracy of both FBDD and MBDD decrease from the cracks at the mid-span to quarter-span.

The literature reviews in this section shows that the dynamical response (e.g., modal frequency, mode shape, damping) can be used as indicator for damage assessment. With various detecting algorithms reviewed here, both modal frequency and mode shape can accurately localize and qualify the damages in structures. However, there are also some limitation. For example, some of proposed modal frequency-based damage detection methods require to know the stiffness matrices of test structures, which is not applicable in practice.

2.5 Summary

In this chapter, the purpose of literature review is to find a suitable method for structural damage detection. Failure mechanism of light poles were first surveyed. Secondly, FE modeling techniques using ABAQUS® for simulating light poles were examined. Thirdly,structural damage detection methodologies using dynamic characteristics(modal frequencies and mode shapes) were reviewed.

From the literature reviews, the following findings are summarized:

- There are three most common/possible damage locations in light poles: (i) pole-to-transverse plate connection, (ii) handhole detail and (iii) anchor bolts;

- The dynamical characteristics of light poles can be obtained by conducting ”pluck test”;
- Structural damages in light poles can be simulated by reducing local materials' properties (i.e. Young's modulus) in FE models;
- Curvatures of mode shapes are more sensitive to damage locations, compared to displacement of mode shapes;
- Changes in modal frequencies and mode shapes are expected while introducing damages into intact structures;
- Both modal frequency and mode shape based damage detection methods can accurately localize and qualify the damages in structures;
- If one pole failed due to fatigue, other similar poles are suspicious to fatigue failure.

Chapter 3

Research Methodology and FE Details

In this chapter, strategies of FE analysis are discussed. The details (e.g., geometry, material properties and boundary conditions) of the original light poles are reported at first. After a review of FE modeling techniques, the intact FE model of the light pole, built by ABAQUS®, is presented. Then the accuracy of the model will be proved by a theoretical calculation of the fundamental frequency, and a convergence study. By introducing artificial damage to the intact modal, damaged light pole models were hence built. The main purpose of this chapter is to discuss the procedure of the FE simulation and data analysis.

3.1 Research Methodology

The purpose of this section is to introduce research strategies and approaches. Selection of parameters is also discussed.

3.1.1 Research approach

As it is reviewed in Chapter 2, any change in structural physical properties (e.g.,mass, stiffness) lead to changes in dynamic responses, such as modal frequency and mode shape. Inversely, changes in dynamical responses can be used as indicators for damage detection.

Therefore, the research approach of this study is to develop damage detection methods by solving the inverse problem: first, discover the relationships among artificial damages and structure's dynamical response by comparing and investigating the different dynamic behaviors of damaged and intact light poles in free vibration; second, use discovered relationships to develop a damage detection method. All dynamic responses of light poles were collected from FE models that built in a commercial package ABAQUS®.

3.1.2 Selection of parameters

Among various dynamic characteristics, two of them were considered as appropriate parameters in this thesis: modal frequencies and corresponding mode shapes. In free vibration, an undamped light pole's modal frequencies and mode shapes are depended on its own geometries, materials' properties and boundary conditions. Meanwhile the effects of external excitations, such as external loadings, do not affect these properties. For example, He and Fu [48] mentioned that an MDoF system can be consider as a collection of separate SDoF systems, which also means the global stiffness is assembled

by stiffnesses of those SDoF system. The lateral stiffness of a fixed-ended, cantilever-beam type SDoF is:

$$k = 3\frac{EI}{h^3} \tag{3.1}$$

where E is Young's modulus, I is Moment of inertia of the SDoF system's cross-section, and h is height of the SDoF system. Thus, the global stiffness matrix of a MDoF system that assembled by numbers of SDoFs can be rewritten as

$$[K] = [N]\frac{EI}{h^3} \tag{3.2}$$

where $[N]$ is a coefficient matrix.

The modal frequency of a MDoF system of rth, mode ω_r, can be calculated by

$$\omega_r^2 = \frac{k_r}{m_r} \tag{3.3}$$

where ω_r is the modal frequency of rth mode, k_r and m_r are the generalized stiffness and mass, also called modal mass and modal stiffness [48]. Structural damage in form of changes in structural physical properties (k_r and m_r), cause the change in modal frequency ω_r. For example, in the equation (3.2), when E (Young's modulus) decreases, the global stiffness decreases with it (I and [N] are constant). As a result, in equation (3.3), when the light poles' stiffness (k_r) decrease, modal frequencies (ω_r) decrease. This result implies that once the physical properties (i.e., mass and stiffness) of a structure are changed with the introductions of damages, modal frequencies of this structure will change in a similar manner. This also happens to mode shapes that correspond to

modal frequencies: once the physical properties are changed, mode shapes will change. Furthermore, no external loading are involved in above equations, which means modal frequency is independent from external loadings. Therefore, by choosing modal frequencies and mode shapes as parameters, one can study the dynamic responses of light pole models while avoiding from simulating external loading conditions in the FE simulations.

In FE simulation, a model without damage will be created with ABAQUS®. Then, damaged models are created by introducing artificial damage to the original model.

3.2 Intact light pole models

3.2.1 Geometry

The example light pole of all FE models is a product from ELEKTROMONTA RZESZW SA, as shown in Figure 3-1. The light pole example have three main components: pole, baseplate and bolts. The light shaft is rigidly connected to the foundation pile (moment connection). The pole shaft is welded to the base plate and the base plate is bolted to the pile with anchor bolts.

- Pole - a pole is vertically assembled to the baseplate. It is round, hollow and taper, with a height of 6 meters. The radius varies from bottom, which is 70 mm, to the top, which is 30 mm. The thickness of the pole body remains 4 mm. A handhole is opened on the pole, with the size of 250*105 mm. The distance between

Table 3.1: Material properties

Part	Pole and Baseplate	Bolts
Density	$7.85 * 10^{-9} ton/mm^3$	$7.85 * 10^{-9} ton/mm^3$
Young's Modulus	$207 * 10^3$ MPa	$207 * 10^3$ MPa
Poisson's ratio	0.3	0.3
Yield stress	450 MPa	250 MPa

handholes' lower edge to the bottom of the pole is 600 mm. No reinforcement is attached to the handhole. The pole body is made with steel, homogeneously. Properties of steel is presented in Table 3.1.

- Baseplate - a homogeneous steel squared plate, with the size of 300*300*30 (mm). At every corner, a round penetrated hole is opened for the installation of a bolt. The radius for each hold is 10 mm. The center of a bolt hole is 50 mm away from two closest edges of baseplate. Figure3-2is the top view of the baseplate. The material's properties are same as pole's, with is presented in Table 3.1

- Bolts - four bolts (Figure 3-3) are installed to fasten the structure to its foundation. The diameter of the head is 30 mm, and the diameter of thread part is 20 mm. The depth of a bolt is 60 mm: 50 mm of threads and 10 mm of head. Bolts' material properties are shown in Table 3.1

Notice that there is no loading applied to light pole structure during free vibration, since external loadings do not affect modal frequency and mode shape of light pole models.

3.2.2 Finite element modeling details of intact model

The FE models are created using ABAQUS®. ABAQUS® provides various families of elements for different usages. For dynamic analysis (i.e., eigenvalue-extraction),

family continuum (solid) is the most appropriate choice. Element C3D8R (Figure 3-4) is selected from this family since it proves the most accurate results.

Meshing methods

In order to improving the quality of FE models, Two sizes of elements are used in the pole's model. Size of the elements in FE models are 30*30*30 (mm). However, because of the existing of handhole and the introduction of artificial damages in lower part of light pole models, mesh reinforcement is required in lower part. Therefore, the element size of lower part is 10*10*10 (mm). Figure 3-5 shows the pole model. The following figures shows the mesh of baseplate and bolts. The element size of baseplate and bolts are identical, which is: 20*20*20 (mm).Figures 3-6 and 3-7 shows the FE models of the bolts and the baseplate.

Interactions and boundary conditions

The pole is welded to the baseplate. In FE models, this contact is simulated by tie constraint. Tie constraint does not allow any displacement or rotation between pole and baseplate. Same constraint is applied between bolts' thread surfaces and bolt-hole's inner surfaces. In the bolt, those regions that pass though the base plate, which are fastened into foundations in, are set as fixed-boundary conditions. Pretension load of a bolt is simulated by applying 'bolt load' on a inner surface inside the bolt. The boundary conditions are shown in Figure 3-8

3.3 Artificially damaged light poles models

3.3.1 Description of artificial damages in light pole models

Three attributes are used to describe artificial damages of light poles,including:

- Damage location - Locations of the damage regions. As it was reviewed in Chapter 2,there are three most common damage locations in light pole structures. As shown in Figures 3-9 and 3-10, from top to bottom: L_1 and L_2 denote damages around the hand hole area, and L_3 denotes the damage at the bottom of the pole. L_1 locates near top edge of the handhole; L_2 locates at the height of lower edge of the handhole;L_3 locates at the bottom of the pole.

- Damage size - The sizes of damaged regions. Different damage sizes can be described by the different proportions of cross-sectional area of a light pole that is damaged. (The heights of those artificially damaged regions are identical (28 mm)). This proportion is define as α^j, where j represents the damage location, j=1,2,3. As an example, if the cross-section's area is A^j, the damage size can be expressed by $\alpha^j A^j$.

- Damage level - The levels of damage in damaged region. This attribute describes severities of the artificial damages. It can be represented by the reduction in material's properties. (i.e., the reduction in Young's modulus.)

3.3.2 Simulation of artificial damages

In previous section, three attributes of artificial damages were discussed. In FE models, the introductions of artificial damages into intact model are accomplished by changing the material's properties base on these three attributes. However, in each damage model, only one damage would be introduced. The cases with multi damages are not included in this work.

Details of simulating damaged FE models are shown in following:

- Damage locations - As it was reported previously, artificial damages are introduced three most common locations. L_1 locates near top edge of the handhole; L_2 locates at the height of lower edge of the handhole;L_3 locates at the bottom of the pole.

- Damages size - Artificial damages can be expressed as $alpha^j A^j$, where A^j is total cross-sectional area at damage location L_j. In FE modeling, the artificial damages have five stages. Start from the intact model, the damage area symmetrically enlarge from $\alpha = 0\%$ to $\alpha = 100\%$ (fully damaged) of cross-sectional area. (20%, 40%,60%,80% and 100 %.) Figure 3-11 shows the cross-sectional view of different damage sizes at location L_3 and L_3.

- Damage level - Five levels of Young's Modulus reduction are designed for simulating different levels of damages. The ratio between intact and damaged model's elastic modulus is β^j, where j is the locations of the damages,varies from 1 to 3. These five levels of reduction in Young's modulus start from $\beta = 90\%$ to

Table 3.2: Reduced Young's modulus of each damage level

β^j	Young's Modulus (Mpa)
0.9	$1.863 * 10^5$
0.7	$1.449 * 10^5$
0.5	$1.035 * 10^5$
0.3	$0.621 * 10^5$
0.1	$0.207 * 10^5$

β = 10%. (90%, 70%,50%,30% and 10%.) Table 3.2 shows the value of Young's modulus in damaged regions after reduction.

3.4 Strategies of dynamic analysis

The first ten modal frequencies of the FE model (including pole, baseplate and bolts), and their corresponding mode shapes were obtained from both intact and damaged models. These dynamic responses were extracted by Lanczos Eigensolver in ABAQUS®. Comparison between intact and damaged models were made based on their dynamic characteristics – modal frequencies and mode shapes. Figure 3-12 shows the strategy of discovering the effects of damages: in each damage scenario, two damage attributes on outer circle keep constant, while the other one attribute varies. Then, investigate the consequences of varying attribute by observing the parameters at center (Δf_i^j) of the circle. Since the general stiffness of a damaged model is reduced, damaged model's modal frequencies will decrease comparing to intact model, and the corresponding mode shapes of damaged models would be different from intact model.

3.5 Verification of the intact FE model

A theoretical calculation was conducted for validating the intact model. The first mode modal frequency of a tapered steel poles was calculated by a theoretical method (Rayleigh's method). The pole has the same size and material properties as FE models. However, it is a pole-only structure with a fix-end boundary condition, and no hand-hole is considered. The following two equations can be used for calculating generalized mass, and generalized stiffness for a system with distributed mass and elasticity [49]:

$$\hat{m} = \int_0^L m(x)[\Psi(x)]^2 dx \tag{3.4}$$

$$\hat{k} = \int_0^L EI(x)[\Psi''(x)]^2 dx \tag{3.5}$$

and the first mode modal frequency can be calculated by:

$$\omega = \sqrt{\frac{k^*}{m^*}} \tag{3.6}$$

where, $\hat{m}$ is generalized mass, $\hat{k}$ is generalized stiffness, ω is the first mode modal frequencies of a SDoF system, x varies from 0 to L, L is the height of the pole, $\Psi(x)$ is the shape function, E is Young's modulus of material, $m(x)$ is mass function, and $I(x)$ is function of moment of inertia.

Three assumed shape functions are provided in *Chopra*'s book [49] for estimating a uniform cantilever beam. *Chopra* points out that because of the properties of Rayleigh's quotient, those three estimates of the natural frequency are higher then its exact value.

Therefore, the lowest value from estimates is the one closest to the true value.

As shown in Figure 3-13, the lowest value of estimation is $4.298Hz$, compare with FE simulation's result (4.236 Hz), only 1.4% of difference. Therefore, the FE model without handhole is validated.

3.6 Summary

Research Methodology and FE Details were introduced in this chapter. The research approach was reported. Light poles' FE models were built base on the information from a real light pole. A convergence study is conducted to achieve the optimal meshing of the FE models. The first mode modal frequencies of a simplified light pole was estimated by Rayleigh's method and then compare to the FE simulation's result, hence the intact FE model is validated. The results of the analysis will be presented in Chapter 4.

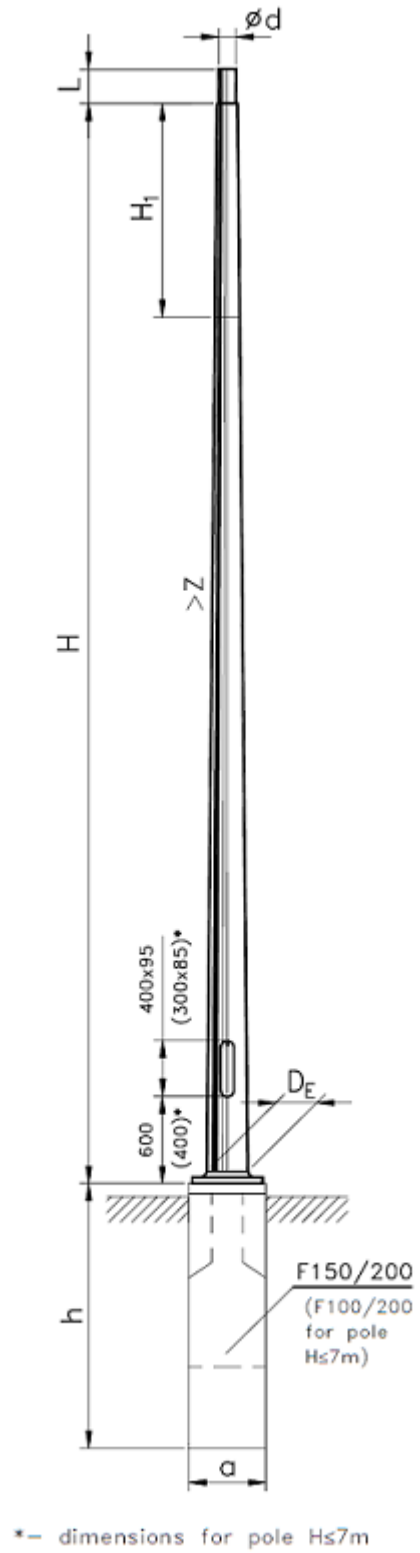

Figure 3-1: Elevation view of the example light pole

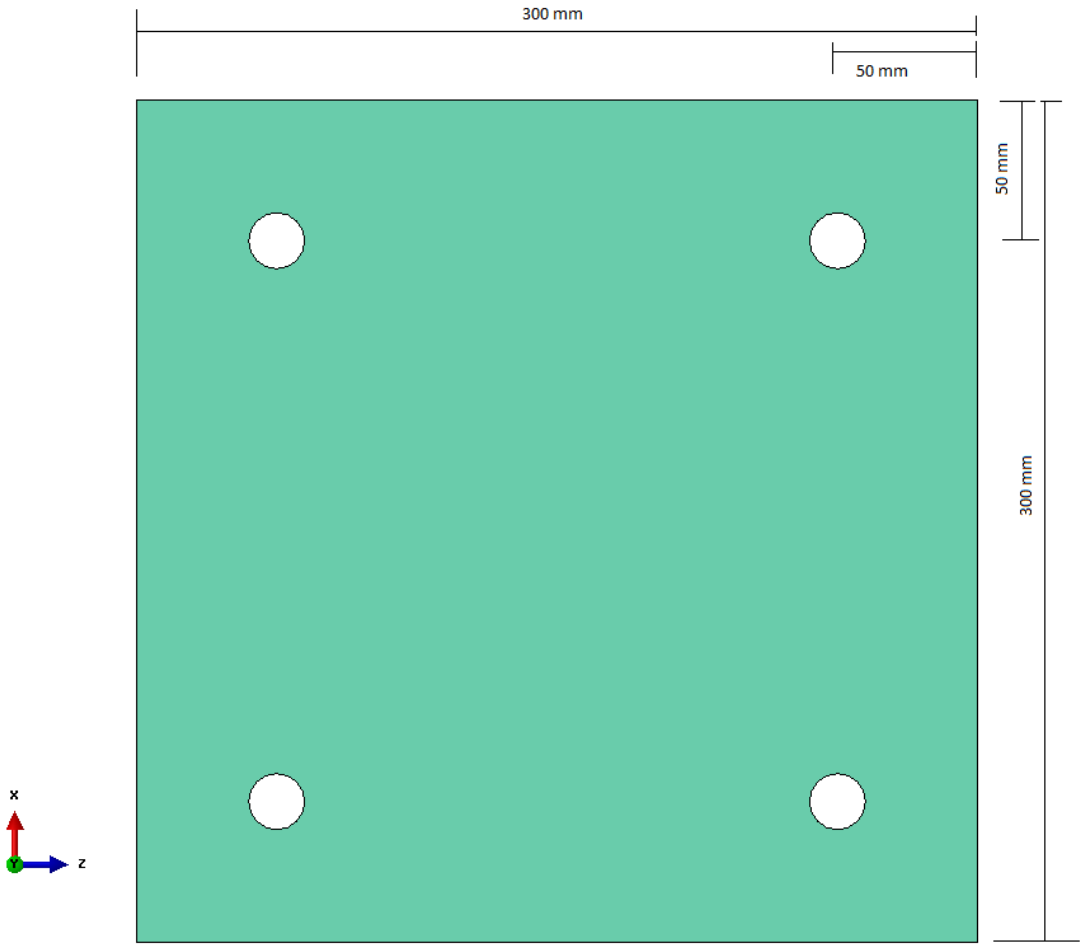

Figure 3-2: Plan view of the baseplate

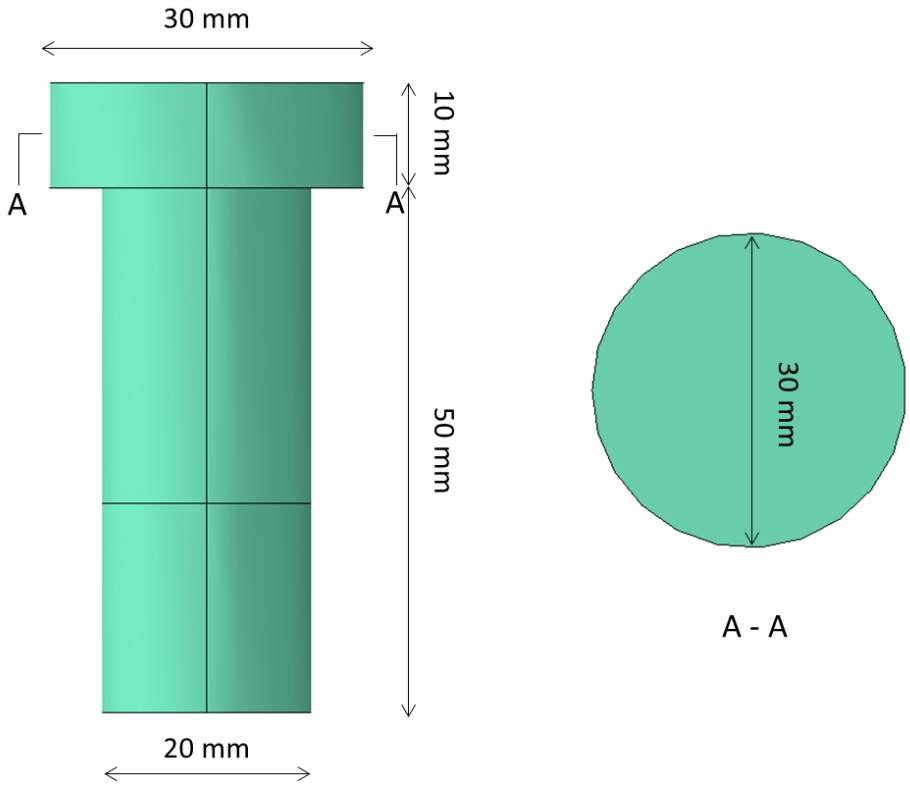

Figure 3-3: Front view of the bolt

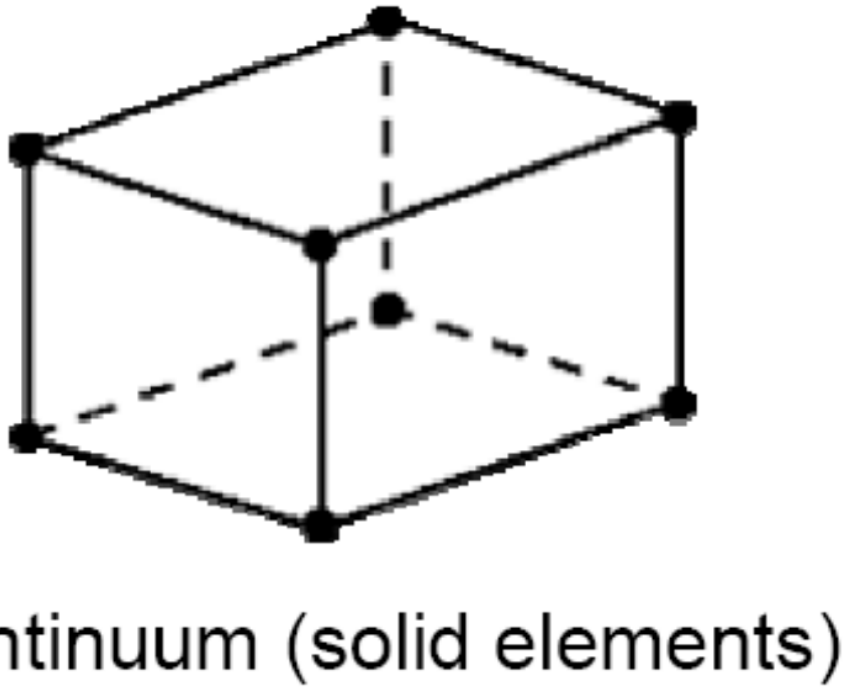

Figure 3-4: C3D8R element

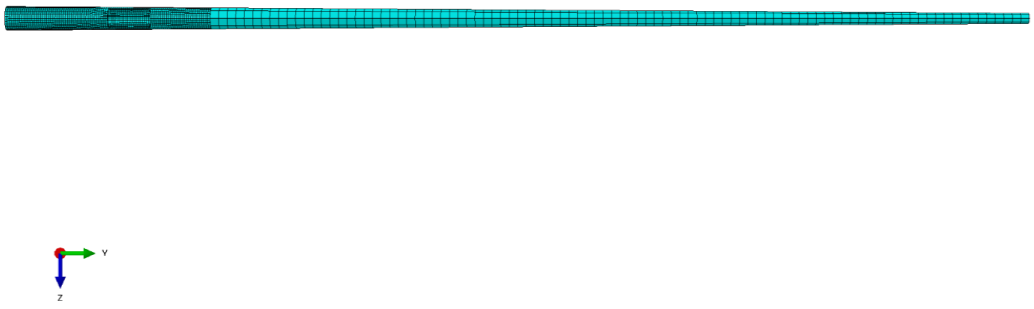

Figure 3-5: FE model of the pole

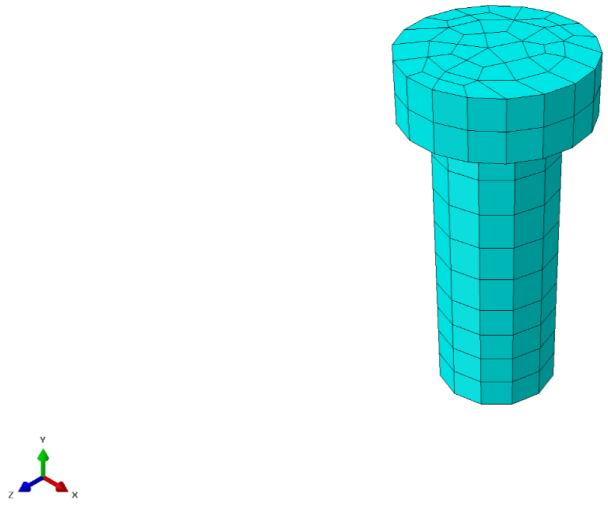

Figure 3-6: FE model of the bolts

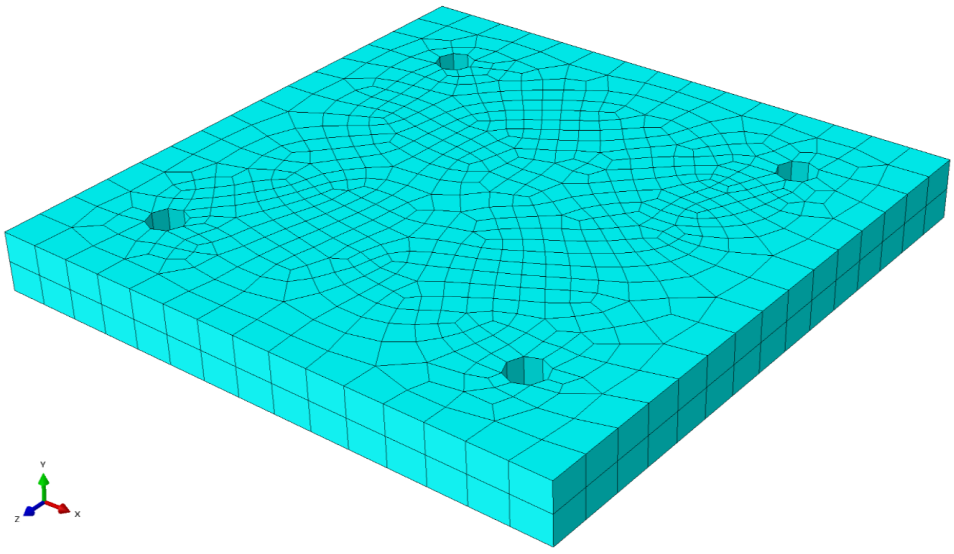

Figure 3-7: FE model of the baseplate

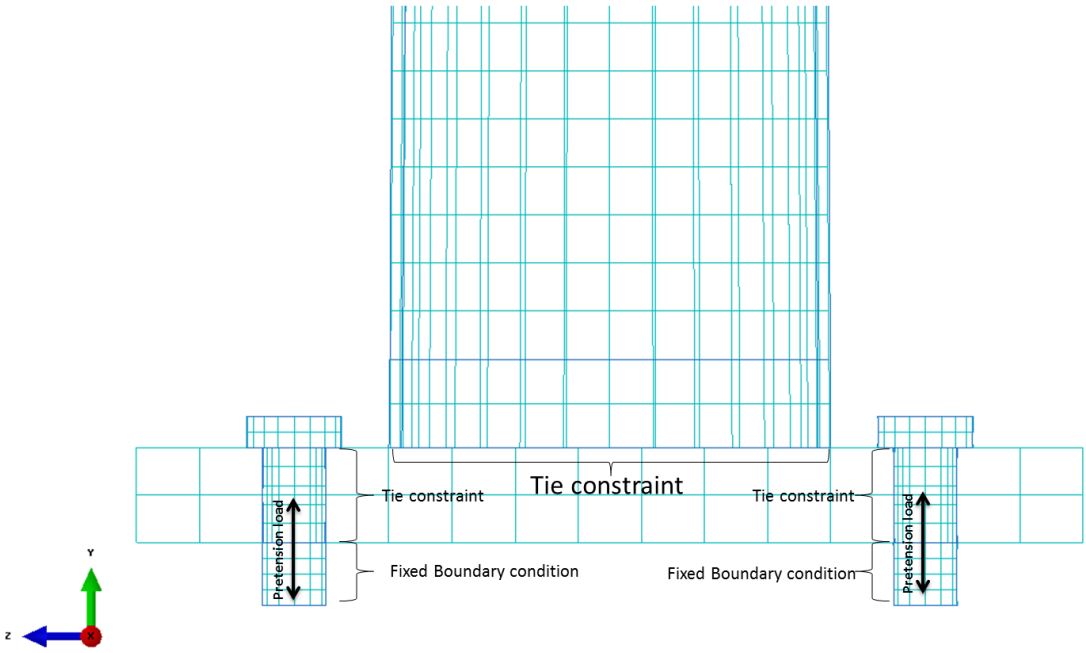

Figure 3-8: Boundary conditions in FE models

Description	Finite Life Constant, $A \times 10^8$ (ksi^3 (MPa^3))	Threshold, $(\Delta F)_{TH}$ (ksi (MPa))	Potential Crack Location	Illustrative Example
SECTION 3 — HOLES AND CUTOUTS				
3.1 Net section of un-reinforced holes and cutouts.	250.0 (85200)	24.0 (165)	In tube wall at edge of unreinforced handhole.	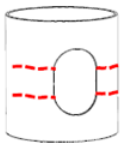
4.6 Full penetration groove-welded tube-to-transverse plate connections welded from both sides with back-gouging (without backing ring).	$K_F \leq 1.6$: 11.0 (3750) $1.6 < K_F \leq 2.3$: 3.9 (1330)	$K_I \leq 3.2$: 10.0 (69) $3.2 < K_I \leq 5.1$: 7.0 (48) $5.1 < K_I \leq 7.2$: 4.5 (31)	In tube wall at groove-weld toe.	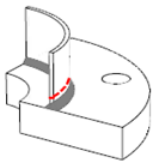

Figure 3-9: Three most common damage locations

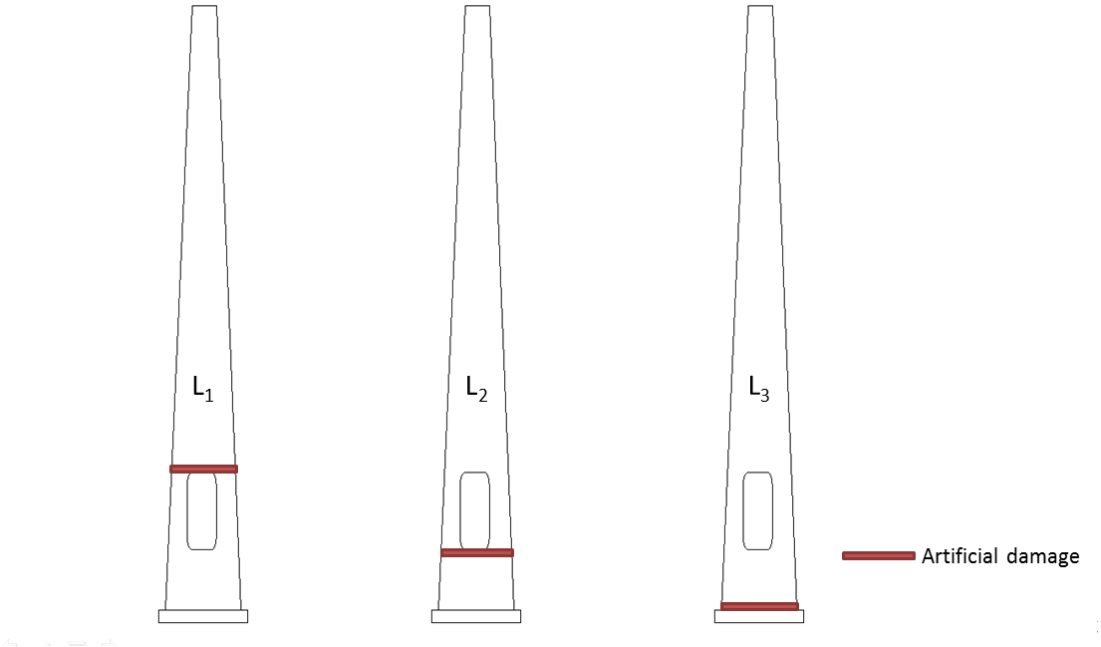

Figure 3-10: Three most common damage locations (2)

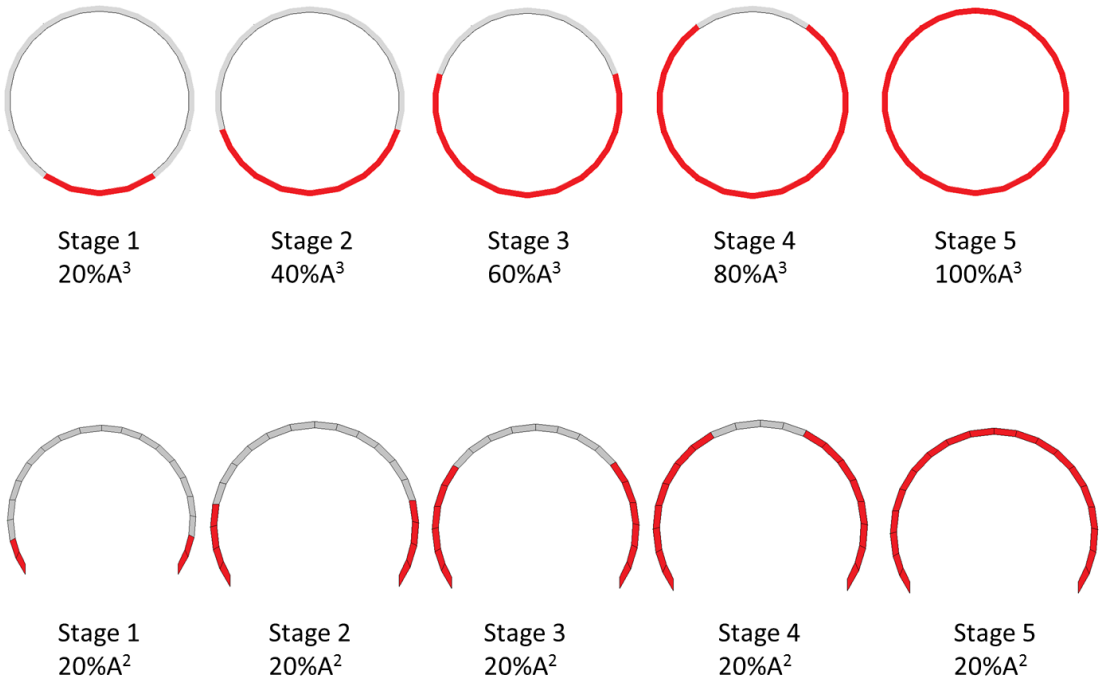

Figure 3-11: Five stages of damages at L_3 and L_2

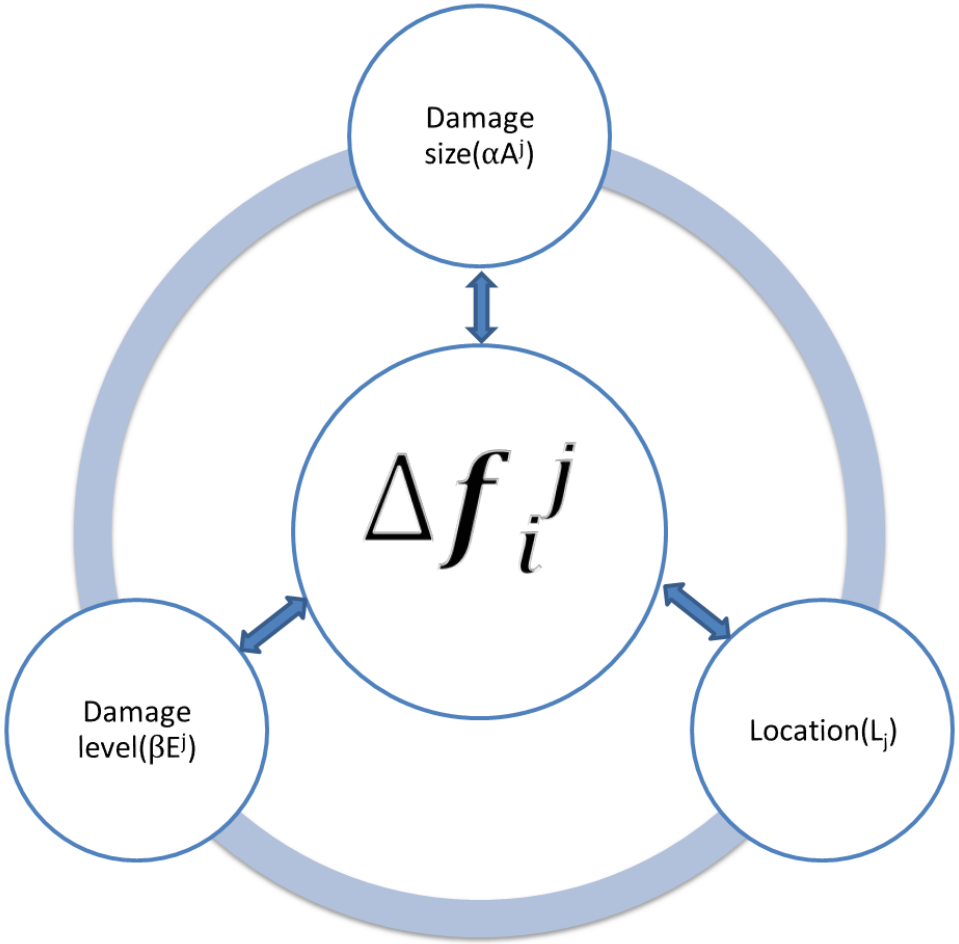

Figure 3-12: Illustration of analysis strategy

Figure 3-13: Estimated first mode modal frequencies using different shape function

Shape function	$\psi(x) := \frac{3x^2}{2\cdot 6000^2} - \frac{x^3}{2\cdot 6000^3}$	$\psi(x) := 1 - \cos\left(\frac{\pi\cdot x}{2\cdot 6000}\right)$	$\psi(x) := \frac{x^2}{6000^2}$
Estimated fundamental frequency (Hz)	4.361	4.298	4.396

Chapter 4

Analysis of FE Simulation Results

4.1 Introduction

In this chapter, results of analysis on modal frequencies and mode shapes of artificial damaged models are reported. FE analysis results of different damage scenarios are also discussed. From the comparison between intact and artificially damaged models, relationships between dynamic response (e.g., modal frequencies and mode shapes) and the damage attributes are discovered. Finally, damage detection methodologies using modal frequencies and mode shapes were suggested to identify damages in the light poles.

4.2 Results on changes in modal frequencies

4.2.1 General approach

As reported in previous chapter, changes in modal frequencies are expected when structural properties (e.g., mass, or stiffness) varies. The introduction of artificial damages to the intact model would reduce the global stiffness of structure. Thus, modal frequencies of models would also alter. By comparing the differences between intact and damaged models.

Three different cases were designed to study the effects of damage attributes. As shown in the Table 4.1, in each case, only one attribute is changed and studied, while the other two are kept constant.

Table 4.1: Considered damage cases

Case	Constant attributes	Varying attribute
Case 1	Damage area(ΔA); Damage level(ΔE)	Damage location(ΔL)
Case 2	Damage level(ΔE); Damage location(ΔL)	Damage area(ΔA)
Case 3	Damage area(ΔA); Damage location(ΔL)	Damage level(ΔE)

4.2.2 Case 1- Varying damage location

Simulations of the intact and damaged light pole models were discussed in Chapter 3. The purpose of this case is to determine the relationship between modal frequencies and damage locations. Thirty derivative damage scenarios (shown in Tables 4.2 and 4.3) were created by ABAQUS®. In each scenario, comparisons are made among models with a damage at different locations, while other damage attributes (damage area (ΔA), and Young's Modulus (ΔE)) remain constant. Those damage locations were shown in

Figure 4-1.

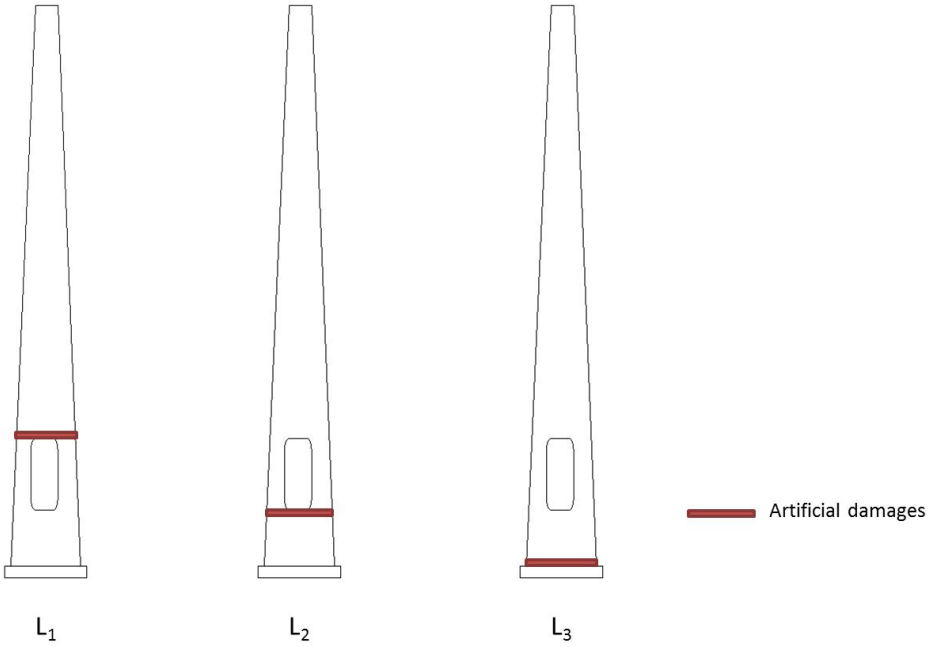

Figure 4-1: Three considered locations of artificial damages

Table 4.2: Derivative damage scenarios in group A

Group A														
ΔE=50% of Youngs modulus														
ΔA=20%			ΔA=40%			ΔA=60%			ΔA=80%			ΔA=100%		
Scenario A-1			Scenario A-2			Scenario A-3			Scenario A-4			Scenario A-5		
L_1	L_2	L_3	L_1	L_2	L_3	L_1	L_2	L_3	L_1	L_2	L_3	L_1	L_2	L_3

The change in modal frequency at *i*th mode is computed using Eq (2.1) from Chapter 2 and Eq (4.2)

$$\frac{\Delta\omega}{\omega} = \frac{\text{uncracked frequency} - \text{cracked frequency}}{\text{uncracked frequency}} \times 100\% = \Delta f_i^j \qquad (4.1)$$

Table 4.3: Derivative damage scenarios in group B

Group B														
Δ A=100% of total area														
ΔE=90%			ΔE=70%			ΔE=50%			ΔE=30%			ΔE=10%		
Scenario B-1			Scenario B-2			Scenario B-3			Scenario B-4			Scenario B-5		
L_1	L_2	L_3	L_1	L_2	L_3	L_1	L_2	L_3	L_1	L_2	L_3	L_1	L_2	L_3

Or,

$$\Delta f_i^j = \frac{(f_i^j|_{intact} - f_i^j|_{damaged})}{f_i^j|_{intact}} \times 100\% \tag{4.2}$$

In order to evaluate sensitiveness of modes, new parameters – 'sensitive modes' and 'insensitive modes' are defined here. Sensitive modes mean that these modes' modal frequencies varies (due to an artificial damage) more than other modes. Those sensitive modes have higher average values in modal frequency differences (Δf_i^j). Sensitive modes are identified using a moving threshold approach. This threshold (t_s) is 1.25 times average modal frequency differences of first ten vibration modes in a damage scenario. Any mode which has an average value of Δf_i^j exceeding this threshold value is considered a sensitive mode.

It is observed that in different damage scenarios, there are some modes always have very low modal frequency difference. Physically, it means that damage attributes' variations (such as changes in damage size) do not effect their modal frequencies as much as other modes. Those models are defined as insensitive modes. Insensitive modes are also identified using a moving threshold approach. The threshold (t_i) is 0.25 times average modal frequency differences of first ten vibration modes in a damage scenario. Any mode which has an average value of Δf_i^j lower than this threshold value is considered

an insensitive mode.

The procedure of finding sensitive modes and insensitive modes for a damage scenario is presented following:

1. Calculate modal frequency difference (Δf_i^j) for each mode using Eq (4.2);
2. Take the average value ($\Delta f_i^j|_{average}$) of first ten modes' modal frequency differences;
3. The threshold value t_s in this damage scenario is $1.25 \times \Delta f_i^j|_{average}$;
4. The modes whose modal frequency differences exceed the threshold are sensitive modes.
5. The threshold value t_i in this damage scenario is $0.25 \times \Delta f_i^j|_{average}$.
6. Find out the modes whose modal frequency differences are lower than the threshold t_i, those modes are insensitive mode.

As an example, Figures 4-2, 4-3, and 4-4 present the sensitive modes for each damage location in damage scenario A-5 (50 % of Young's modulus, 100% of cross-section are damaged). The thresholds t_s are : L_1 – 0.7891%, L_2 – 0.7637% and L_3 – 0.5286%. The sensitive modes for each location are: L_1 – 1st, 7th; L_2 – 1st,7th; L_3 – 10th. The threshold values t_i for each damage location are: L_1 – 0.1578%, L_2 – 0.1527% and L_3 – 0.1057%. The insensitive modes for each location are: L_1 – 6th; L_2 – 8th and 10th; L_3 – 7th.

Tables 4.4, 4.6 and 4.8 list the sensitive modes for each damage location. Tables 4.5, 4.7 and 4.9 list the insensitive modes for each damage location. In these tables, α

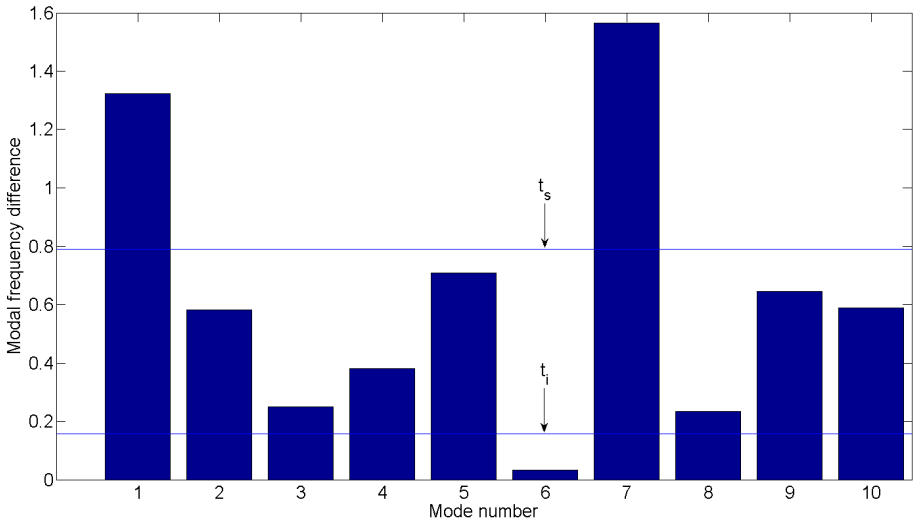

Figure 4-2: Modal frequency differences at location L_1

represents the ratio of cross-sectional area that is damaged, and β represents the ration of Young's modulus.

It is found that the combination of sensitive modes and insensitive modes is unique for

Table 4.4: Sensitive modes for damage location L_1

Damage location	α	Sensitive modes	β	Sensitive modes
L_1	20%	1,5,7	90%	1,7
	40%	1,7	70%	1,7
	60%	1,7	50%	1,7
	80%	1,7	30%	1,7
	100%	1,7	10%	1,7
	Mutual sensitive modes = 1,7			

each damage location. Therefore, one can locate a damage in a light pole by knowing the corresponding combination of sensitive modes and insensitive modes. (as shown in Table 4.10.)

Table 4.5: Insensitive modes for damage location L_1

Damage location	α	Insensitive modes	β	Insensitive modes
L_1	20%	6	90%	6
	40%	6	70%	6
	60%	6	50%	6
	80%	6	30%	6
	100%	6	10%	6
	Mutual sensitive modes = 6			

Table 4.6: Sensitive modes for damage location L_2

Damage location	α	Sensitive modes	β	Sensitives modes
L_2	20%	1,7,9	90%	1,7
	40%	1,7	70%	1,7
	60%	1,5,7	50%	1,7
	80%	1,7	30%	1,7
	100%	1,7	10%	1,2,7
	Mutual sensitive modes = 1,7			

Table 4.7: Insensitive modes for damage location L_2

Damage location	α	Insensitive modes	β	Insensitives modes
L_2	20%	8,10	90%	8,10
	40%	8,10	70%	8,10
	60%	8,10	50%	8,10
	80%	8,10	30%	8,10
	100%	8,10	10%	8,10
	Mutual insensitive modes = 8,10			

Table 4.8: Sensitive modes for damage location L_3

Damage location	α	Sensitive modes	β	Sensitives modes
L_3	20%	1,3,6,8,10	90%	9,10
	40%	8,9,10	70%	9,10
	60%	2,4,9,10	50%	10
	80%	2,4,9	30%	10
	100%	10	10%	2,4,10
	Mutual sensitive modes = 10			

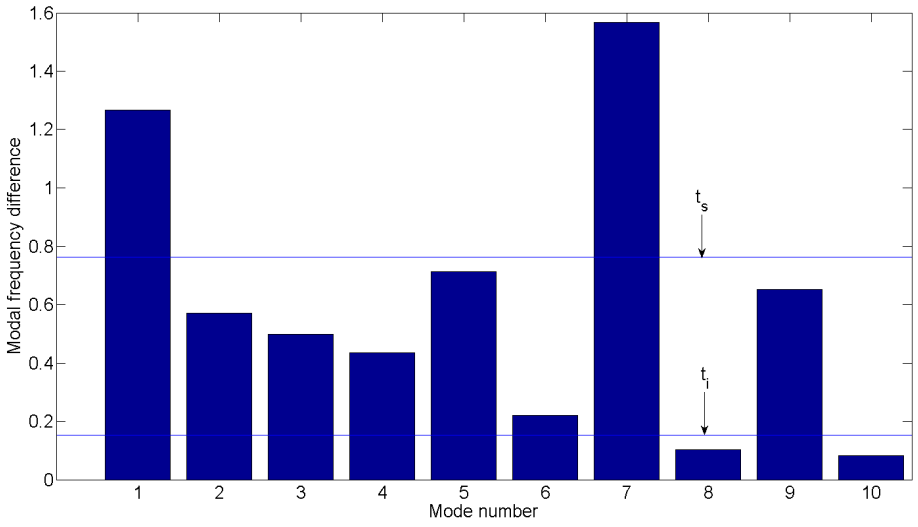

Figure 4-3: Modal frequency differences at location L_2

Table 4.9: Insensitive modes for damage location L_3

Damage location	α	Insensitive modes	β	Insensitives modes
L_3	20%	7	90%	7
	40%	7	70%	7
	60%	7	50%	7
	80%	7	30%	7
	100%	7	10%	7
	Mutual sensitive modes = 7			

4.2.3 Case 2- Varying damaged area

The objective of Case 2 is to study the effects of a varying damage area in modal frequencies. In this case, damage attributes-location (ΔL) and Young's modulus (ΔE) are constant. Tables 4.11, 4.12 and 4.13 display the modal frequency differences of damage scenarios with different damage sizes.

For each damage location, a linear model is developed based on the largest coefficient of determination – R^2 value of the mode. (R^2 value indicates how well data points fit a statistical model.)

Table 4.10: Sensitive and insensitive modes of each location

Location	Sensitive modes	Insensitive modes
L_1	1, 7	6
L_2	1, 7	8, 10
L_3	9 or 10	7

Table 4.11: Modal frequencies' differences for location L_1 (with different damage sizes)

	α=20%	α=40%	α=60%	α=80%	α=100%	R^2
Mode 1	**0.863412**	**0.996987**	**1.022123**	**1.126469**	**1.324054**	0.935873
Mode 2	0.241562	0.400602	0.50788	0.568145	0.581398	0.89757
Mode 3	0.140152	0.176225	0.180956	0.204019	0.250736	0.933339
Mode 4	0.302525	0.328308	0.348935	0.372427	0.380448	0.976376
Mode 5	0.544283	0.659928	0.69678	0.704295	0.709387	0.734539
Mode 6	0.012415	0.023928	0.027765	0.029571	0.032957	0.870419
Mode 7	**0.990841**	**1.385948**	**1.539601**	**1.561405**	**1.565941**	0.731315
Mode 8	0.188398	0.206057	0.217988	0.225744	0.233619	0.965149
Mode 9	0.480504	0.578081	0.616426	0.632013	0.644795	0.831503
Mode 10	0.481485	0.520606	0.537909	0.560479	0.589067	0.984081

Table 4.12: Modal frequencies' differences for location L_2 (with different damage sizes)

	α=20%	α=40%	α=60%	α=80%	α=100%	R^2
Mode 1	**0.834183**	**0.936483**	**0.960159**	**1.063043**	**1.267059**	0.914542
Mode 2	0.143036	0.356591	0.496127	0.558642	0.570896	0.871481
Mode 3	0.360138	0.390888	0.402124	0.436423	0.499107	0.929879
Mode 4	0.111155	0.297368	0.399929	0.429723	0.435453	0.815337
Mode 5	0.490461	0.638109	0.698234	0.70769	0.712054	0.74915
Mode 6	0.176974	0.188486	0.19729	0.207448	0.220089	0.996622
Mode 7	**1.361803**	**1.477262**	**1.524235**	**1.554527**	**1.566966**	0.860952
Mode 8	0.07493	0.090799	0.10094	0.103327	0.103804	0.819974
Mode 9	0.548153	0.586706	0.611749	0.634715	0.651029	0.975287
Mode 10	0.021817	0.054919	0.066204	0.07147	0.082755	0.883046

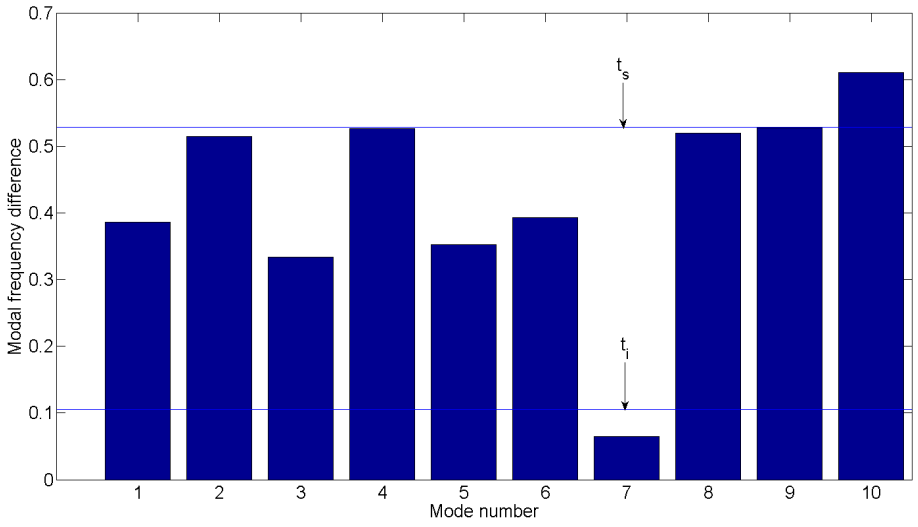

Figure 4-4: Modal frequency differences at location L_3

At location L_1, with R^2 =0.9841,

$$\alpha^1 = 0.0255\Delta f_{10}^1 + 0.4614 \tag{4.3}$$

At location L_2, with R^2 =0.9966,

$$\alpha^2 = 0.0526\Delta f_6^2 + 0.1665 \tag{4.4}$$

At location L_3, with R^2 =0.9750,

$$\alpha^3 = 0.6858\Delta f_4^3 - 0.1251 \tag{4.5}$$

where α^j is the percentage of the cross-sectional area reduction at location j; Δf_i^j is the modal frequency difference in ith mode at location L_j; i is mode number and j represents damage location.

Table 4.13: Modal frequencies' differences for location L_3 (with different damage sizes)

	α=20%	α=40%	α=60%	α=80%	α=100%	R^2
Mode 1	0.099962	0.169526	0.178294	0.223306	0.385817	0.853656
Mode 2	0.022006	0.137035	0.31458	0.47112	0.514131	0.971786
Mode 3	0.087521	0.149022	0.15671	0.196923	0.334118	0.861758
Mode 4	0.018908	0.117458	0.295077	0.473841	0.526554	0.974984
Mode 5	0.00994	0.052368	0.161224	0.304993	0.352754	0.967809
Mode 6	0.102031	0.175394	0.18668	0.235439	0.393451	0.873225
Mode 7	0.012439	0.03556	0.042437	0.055461	0.06468	0.960327
Mode 8	0.13065	0.227534	0.245073	0.313202	0.519617	0.882234
Mode 9	0.037825	0.209701	0.39228	0.490272	0.527162	0.942374
Mode 10	**0.157235**	**0.264065**	**0.28513**	**0.379922**	**0.610885**	0.893592

4.2.4 Case 3-Varying material property

The objective in Case 3 is to study the effects of varying Young's modulus of materials at a given damage location and a given damage region. Similar procedure in Case 2 is applied in Case 3. In a damage region, damage attributes location (L_j) and damaged region's area (αA) were kept constant while material's property (Young's modulus) is changing.

Tables 4.14, 4.15 and 4.16 display the modal frequency differences of damage scenarios with different damage levels (reduction in Young's modulus).

Figures B.4, B.5 and B.6 show the best-fit models using non-linear equations. The results are in the following:

Table 4.14: Modal frequencies' differences for location L_1 (with different damage levels)

	β=90%	β=70%	β=50%	β=30%	β=10%	R^2
Mode 1	**0.1593**	**0.5945**	**1.3241**	**2.8647**	**9.0433**	0.9905
Mode 2	0.0663	0.2531	0.5814	1.3188	4.6494	0.9911
Mode 3	0.0302	0.1129	0.2507	0.5411	1.6653	0.9903
Mode 4	0.0470	0.1742	0.3804	0.7936	2.2552	0.9891
Mode 5	0.0943	0.3380	0.7094	1.3785	3.2497	0.9845
Mode 6	0.0045	0.0156	0.0330	0.0657	0.1781	0.9892
Mode 7	**0.2135**	**0.7576**	**1.5659**	**2.9681**	**6.6281**	0.9821
Mode 8	0.0296	0.1081	0.2336	0.4796	1.3230	0.9887
Mode 9	0.0917	0.3199	0.6448	1.1733	2.4095	0.9774
Mode 10	0.0737	0.2716	0.5891	1.2173	3.3478	0.9887

Table 4.15: Modal frequencies' differences for location L_2 (with different damage levels)

	β=90%	β=70%	β=50%	β=30%	β=10%	R^2
Mode 1	**0.151989**	**0.567619**	**1.267059**	**2.756839**	**8.838135**	0.99061
Mode 2	0.064767	0.247813	0.570896	1.301582	4.664689	0.991111
Mode 3	0.061501	0.226491	0.499107	1.056167	3.089851	0.990059
Mode 4	0.053286	0.1971	0.435453	0.930494	2.841329	0.990285
Mode 5	0.09334	0.33651	0.712054	1.406166	3.431288	0.985804
Mode 6	0.027991	0.102031	0.220089	0.451238	1.216922	0.988532
Mode 7	**0.209992**	**0.750265**	**1.566966**	**3.021252**	**6.939691**	0.983567
Mode 8	0.013721	0.049158	0.103804	0.20558	0.518304	0.986729
Mode 9	0.090095	0.317669	0.651029	1.21768	2.63789	0.980662
Mode 10	0.010532	0.037616	0.082755	0.174538	0.545433	0.990655

Table 4.16: Modal frequencies' differences for location L_3 (with different damage levels)

	β=90%	β=70%	β=50%	β=30%	β=10%	R^2
Mode 1	0.043551	0.167187	0.385817	0.884749	3.217189	0.991071
Mode 2	0.058265	0.222807	0.514131	1.17605	4.237831	0.99118
Mode 3	0.037847	0.144883	0.334118	0.759896	2.672943	0.991251
Mode 4	0.060161	0.229759	0.526554	1.188328	4.041116	0.991258
Mode 5	0.040973	0.154921	0.352754	0.784786	2.527705	0.991293
Mode 6	0.044921	0.171331	0.393451	0.890739	3.059121	0.991332
Mode 7	0.007756	0.028975	0.06468	0.13858	0.405351	0.990236
Mode 8	0.059657	0.227056	0.519617	1.1669	3.856378	0.991361
Mode 9	0.060583	0.230588	0.527162	1.181933	3.8882	0.991322
Mode 10	**0.070718**	**0.268579**	**0.610885**	**1.351168**	**4.1814**	0.991092

At location L_1, with highest R^2 =0.9911 in mode 2,

$$\beta^1 = -0.195 \ln(f_2^1) + 0.39 \tag{4.6}$$

At location L_2, with highest R^2 =0.9914 in mode 2,

$$\beta^2 = -0.194 \ln(f_2^2) + 0.3879 \tag{4.7}$$

At location L_3, with highest R^2 =0.9914 in mode 8,

$$\beta^3 = -0.199 \ln(f_8^3) + 0.3628 \tag{4.8}$$

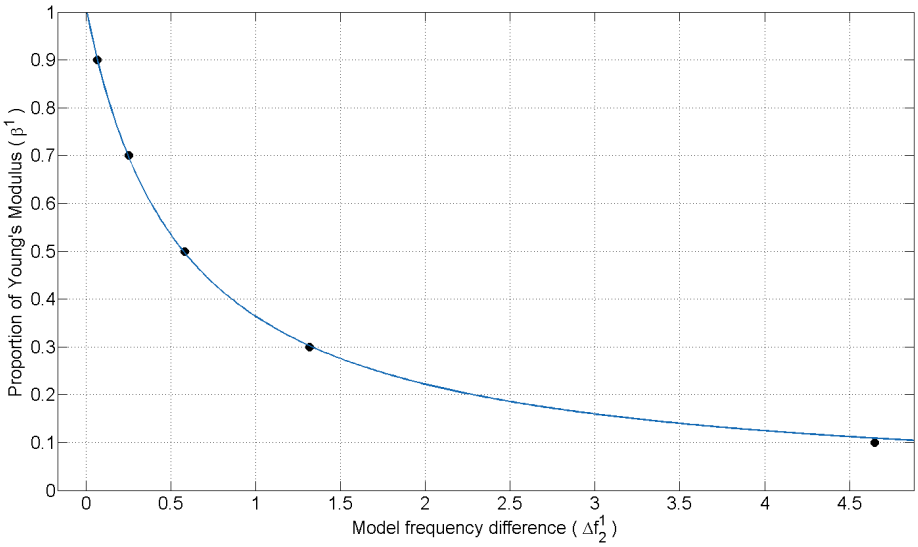

Figure 4-5: Best-fit mode at location L_1

4.2.5 The validation of sensitive modes

In previous sections, sensitive modes were used to identify the damage location in light pole models. A unknown light pole's sensitive modes are identified using a moving threshold approach. This threshold is 1.25 multiplies average modal frequency differences of first ten vibration modes. Sensitive modes are those vibration modes of which modal frequency differences exceed threshold. The use of sensitive modes in damage detection is validated by a theoretical derivation.

Gudmunson [42] proposed an equation (Eq (4.9)) which relates fractional changes in modal strain energy and in fractional changes modal frequency:

$$\frac{\delta W_i}{W_i} = \frac{\delta \omega_i^2}{\omega^2} \tag{4.9}$$

where W_i is the ith modal strain energy of the initial structure, δW_i is the loss in the ith

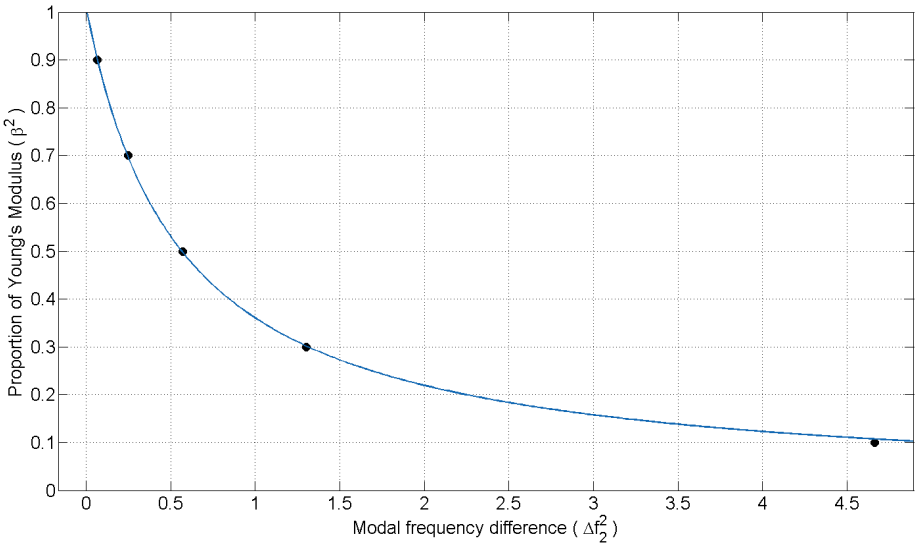

Figure 4-6: Best-fit mode at location L_2

modal strain energy after damage, and $\frac{\delta\omega_i^2}{\omega^2}$ is the fractional change in the *i*th eigenvalue (modal frequency difference) due to the introduction of damage. For intact structures, W_i and ω^2 keep constant. In Eq (4.9), increasing δW_i results increment of $\delta\omega_i^2$. Thus, if in *i*th mode the values of $\delta\omega_i^2$ is maximum among all modes, δW_i must be the maximum among all modes.

Kim *et. al.* [18] proposed the following equation to compute δW_i of a simple supported beam structure:

$$\delta W_i = \left(\frac{\pi t(1-\nu^2)}{2E} F^2 \sigma_k^2 a_k^2 \right)_i \tag{4.10}$$

in which, for the *i*th mode, $a_k^2 = a(x_k)$ represents the damage size (depth) at location x_k and $\sigma_k^2 = \sigma(x_k)$ represents the maximum flexural stress at location x_k along the beam's longitudinal axis, t is the beam thickness, E is Young's modulus, ν is Poisson's ratio and F is a geometrical factor depending on the dimensionless crack-length/beam-depth ratio a/H. For an unknown beam, values of π, t, ν, E, F, a_k are identical, whether it is

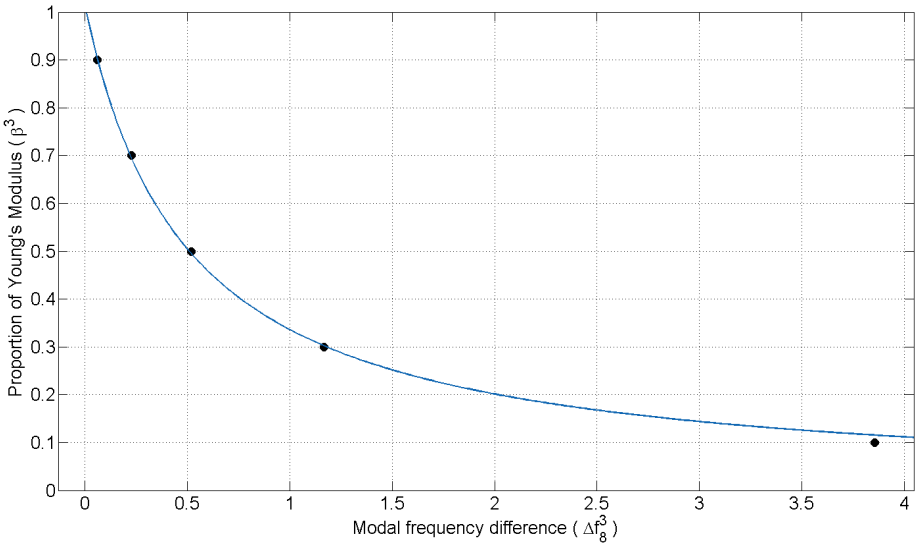

Figure 4-7: Best-fit mode at location L_3

intact or damaged. Therefore, in Eq (4.10) increasing value of σ_k^2 results increment in δW_i. As it was described above, the increment of δW_i results increase of $\delta\omega_i^2$. It means $\delta\omega_i^2$ increases when σ_k^2 increasing. As a result, one can find the most sensitive modes (the modes which has largest modal frequency difference) by checking the maximum value of $\Delta\sigma_k^2$ (difference between intact and damaged structures).

For a Euler-Bernoulli beam, the σ can be computed by the following steps:

1. For an Euler-Bernoulli beam, its bending moment at location x is:

$$M(x) = -EI\frac{d^2\phi(x)}{dx^2} = -EI\phi''(x) \tag{4.11}$$

where I is moment of inertia of the beam cross-section at location x, $\phi(x)$ is the displacement of the beam and $\phi''(x)$ is the curvature.

2. The longitudinal stress of an arbitrary point m on this cross-section is:

$$\sigma_m = \frac{M(x)c_m}{I} \tag{4.12}$$

where σ_m is longitudinal stress of an arbitrary point m, and c_m is the distance between point m and cross-sectional neutral axis.

3. Substitute Eq (4.11) into Eq (4.12):

$$\sigma_m = -c_m E\phi''(x) \tag{4.13}$$

4. Then, difference between intact and damaged structures $\Delta\sigma_m$ is (symbol "*" indicates damaged structures):

$$\Delta\sigma_m = \frac{\sigma_m - \sigma_m^*}{\sigma_m} = \frac{-c_m E\phi''(x) - (-c_m E^*\phi''^*(x))}{-c_m E\phi''(x)} = 1 - j\frac{\phi''^*}{\phi''} \tag{4.14}$$

where E^* is Young's modulus of damaged materials, and j is the ratio between E and E^* ($E = jE^*$). Therefore, maximum $\Delta\sigma$ can be obtained by finding minimum value of ϕ''^*/ϕ''.

Central difference approximation was used to compute the curvature at location x, which is:

$$\phi''(x)_n = \frac{\phi(x)_{n+1} - 2\phi(x)_n + \phi(x)_{n-1}}{d^2} \tag{4.15}$$

where n represent node n on beams, $\phi''(x)_n$ is the curvature of beam at node n (located

at x) and d is the distance between two nodes which is constant. Then,

$$\frac{\phi''^{*}(x)_n}{\phi''(x)_n} = \frac{\phi^{*}(x)_{n+1} - 2\phi^{*}(x)_n + \phi^{*}(x)_{n-1}}{\phi(x)_{n+1} - 2\phi(x)_n + \phi(x)_{n-1}} \tag{4.16}$$

Let $\phi^{*}(x)_n = \phi(x)_n + \delta_n$, where δ_n is the differential displacement between $\phi^{*}(x)_n$ and $\phi(x)_n$, Eq (4.16) is equal to:

$$\begin{aligned} \frac{\phi''^{*}(x)_n}{\phi''(x)_n} &= \frac{(\phi(x)_{n+1} + \delta_{n+1}) - 2(\phi(x)_n + \delta_n) + (\phi(x)_{n-1} + \delta_{n-1})}{\phi(x)_{n+1} - 2\phi(x)_n + \phi(x)_{n-1}} \\ &= 1 + \frac{\delta_{n+1} - 2\delta_n + \delta_{n-1}}{\phi(x)_{n+1} - 2\phi(x)_n + \phi(x)_{n-1}} \end{aligned} \tag{4.17}$$

$\phi(x)_{n+1}$, $\phi(x)_n$ and $\phi(x)_{n-1}$ are displacements of given nodes on intact structure, which are constant values.

By finding minimum value of $\delta_{n+1} - 2\delta_n + \delta_{n-1}$, one can obtain the minimum value of $\phi''^{*}(x)_n/\phi''(x)_n$. Hence the maximum value of $\Delta\sigma_m$ in Eq (4.14) can be found. As it is described above, a maximum $\Delta\sigma_m$ results maximum $\delta\omega^2$, which indicates the most sensitive mode. Inversely, the most sensitive mode should have lowest value of $\delta_{n+1} - 2\delta_n + \delta_{n-1}$.

Damage scenario A-5 was used as an example. The most sensitive mode for three different damage locations are: L_1–7th Mode; L_2–7th Mode; and L_3–10th mode. The value of $\delta_{n+1} - 2\delta_n + \delta_{n-1}$ for each vibration mode is calculated by taking average value $\delta_{average}$ from 250 nodes distributed on light pole models (as shown in Fig.4-8). Figures 4-9, 4-10 and 4-11 show the average values of $\delta_{n+1} - 2\delta_n + \delta_{n-1}$ of first ten modes. From those figures, the lowest average values of $\delta_{n+1} - 2\delta_n + \delta_{n-1}$ among first

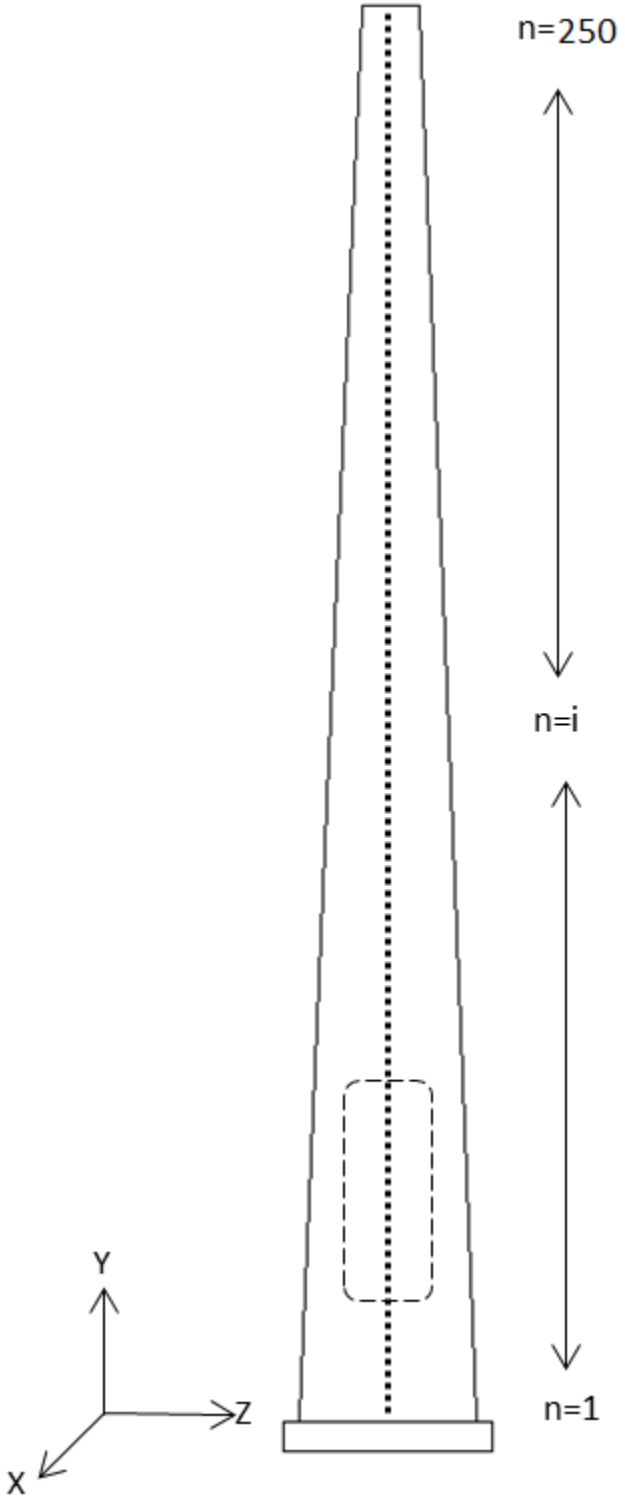

Figure 4-8: 250 nodes distributed on light pole models

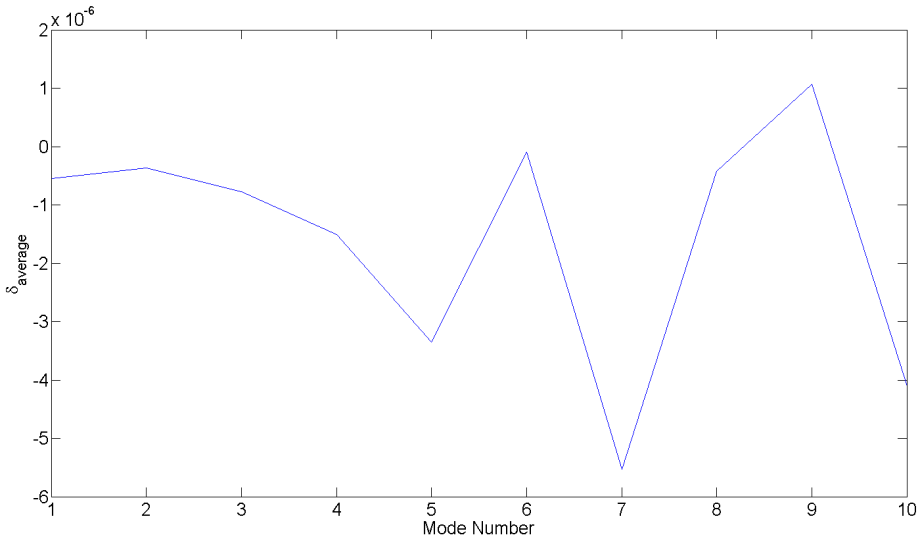

Figure 4-9: $\delta_{average}$ for damage location L_1

Table 4.17: Most sensitive mode and minimum $\delta_{average}$

	Most sensitive mode	Minimum $\delta_{average}$
L_1	7th mode	7th mode
L_2	7th mode	7th mode
L_3	10th mode	10th mode

ten modes occur in: L_1–7th Mode; L_2–7th Mode; and L_3–10th mode, which matches the results of most sensitive modes. As shown in table 4.17.

4.3 Result on blind-test

In some special cases, information from intact structures is unavailable. 'Blind-test' is the damage detection method used in this situation. The objective of this section is to find out a damage detection method without knowing the intact light pole.

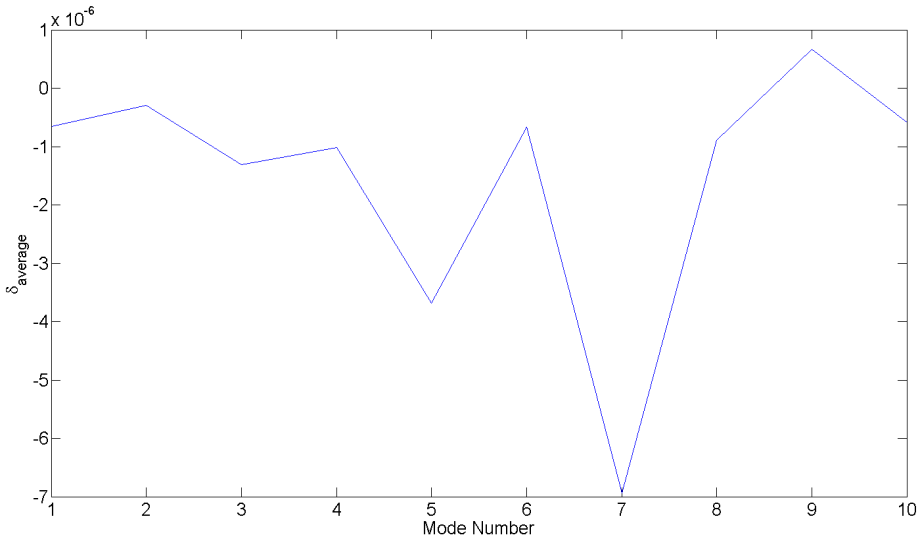

Figure 4-10: $\delta_{average}$ for damage location L_2

4.3.1 Strategy of blind-test

Artificial damages with different attributes (ΔA, ΔL and ΔE) cause different reductions in stiffness of light poles, which lead to modal frequency differences between different damaged models.

However, the problem with blind-test is: intact model is unavailable so that modal frequency difference can not be computed. Thus, sensitive modes and insensitive modes can not be identified.

Therefore, the strategy for blind-test is: use an unknown light pole as the baseline to calculate modal frequency difference instead of intact light poles.

Two assumptions were made for blind-test. 1) Usually light poles are installed plurally in similar environment, so that one can alway obtain modal frequencies from a set of light pole with similar condition. 2) In FE simulation, similar conditions of light poles are considered as damages with same damage location (ΔL), same damage size (ΔA)

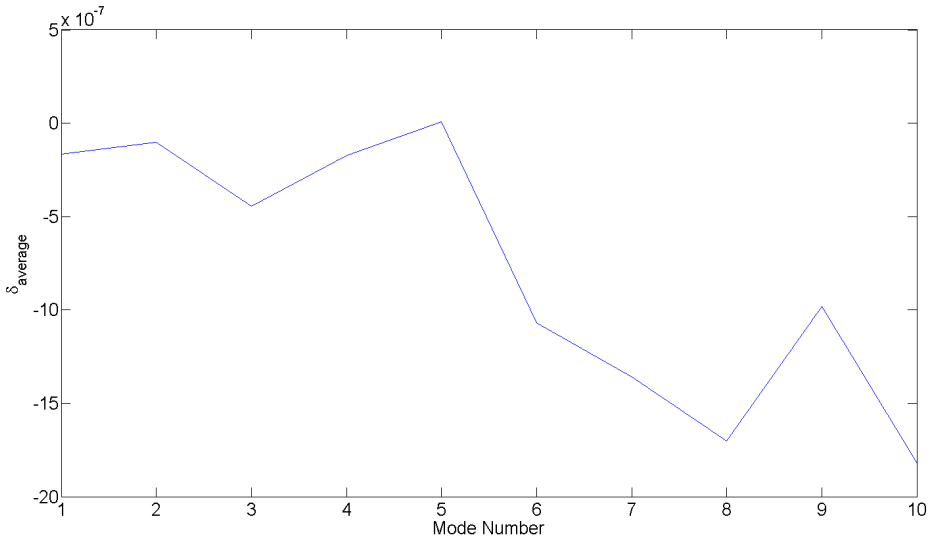

Figure 4-11: $\delta_{average}$ for damage location L_3

and different damage levels (ΔE).

In blind-test, sensitive modes and insensitive modes of light poles can be identified by following steps:

1. Obtain a set of data (i.e., modal frequencies) from light poles in similar conditions.

2. Select an arbitrary unknown light pole as baseline instead of intact light pole.

3. Compute the modal frequency differences for other unknown light poles using Eq (4.18).

$$\Delta f_i^j = \left| \frac{(f_i^j|_{baseline} - f_i^j|_{damaged})}{f_i^j|_{baseline}} \right| * 100\% \tag{4.18}$$

4. Use same moving thresholds t_s (1.25 times average modal frequency differences of first ten vibration modes) and t_i (0.25 times average modal frequency differences of first ten vibration modes) to determine the sensitive/insensitive modes.

For demonstration, above procedures were conducted on three sets of damaged models (15 in total). In a set of models, damage locations and damage sizes keep constant, and damage levels varying from 90% of Young's modulus to 10%. Each time, one of these models was considered as baseline model, sensitive and insensitive modes were hence identified. Tables 4.18, 4.19 and 4.20 list the identified sensitive modes and insensitive modes for three different damage locations.

Table 4.18: Blind-test results for models with damages at L_1

Damage Location	Baseline model	Mutual sensitive modes	Mutual Insensitive modes
L1	90%E	1,7	6
	70%E	1,7	6
	50%E	1,7	6
	30%E	1,7	6
	10%E	1,2,7	6
		Mutual sensitive modes=1,7	Mutual insensitive modes=6

Table 4.19: Blind-test results for models with damages at L_2

Damage Location	Baseline model	Mutual sensitive modes	Mutual Insensitive modes
L2	90%E	1,7	8
	70%E	1,7	8
	50%E	1,7	8
	30%E	1,7	8
	10%E	1,2,7	8
		Mutual sensitive modes=1,7	Mutual insensitive modes=8

It is found that the combination of sensitive modes and insensitive modes are unique for each damage location, no matter which model is the baseline. In addition, these combinations are similar to those combinations for basis-test (tests with knowing intact models). Table 4.21 list the combination of sensitive modes and insensitive modes for each damage location.

Table 4.20: Blind-test results for models with damages at L_3

Damage Location	Baseline model	Mutual sensitive modes	Mutual Insensitive modes
L3	90%E	10	7
	70%E	10	7
	50%E	10	7
	30%E	10	7
	10%E	2,4,10	7
		Mutual sensitive modes=10	Mutual insensitive modes=7

Table 4.21: Combination of sensitive and insensitive modes for blind-test

Location	Sensitive modes	Insensitve modes
L1	1,7	6
L2	1,7	8
L3	10	7

4.4 Result on changes in mode shapes

The objective in this section is to use a different parameter–mode shape to investigate the effects of artificial damages. To be specific, the parameter used in this section is changes in mode shapes' curvature. As it is reported in Chapter 2, curvatures of mode shapes are more sensitive to damage locations, comparing with displacement of mode shapes.

As examples, fifteen damage scenarios were introduced to intact model. Those scenarios were combined with three different damage locations and five different damage area, with 50% of Young's modulus in damaged region. 250 nodes (as shown in Figure 4-8) were set on light pole models to record the displacements of mode shapes, and for the calculation of mode shape curvatures.

The mode shape study in this example is second mode, in which one can minimize the

possible effects of handhole. The displacement of mode shapes considered is only on Z-axis direction. (Figures 4-12 and 4-13.) The curvature of mode shape at each node was calculated by central difference equation, Eq (4.19)

$$\phi_n'' = \frac{\phi_{(n+1)} - 2\phi_n + \phi_{n-1}}{d^2} \tag{4.19}$$

where ϕ_n'' is the curvature of mode shape at node n, ϕ_n is the displacement of mode shape at node n and d is the distance between two nodes. Figure 4-14 to Figure 4-18 shows

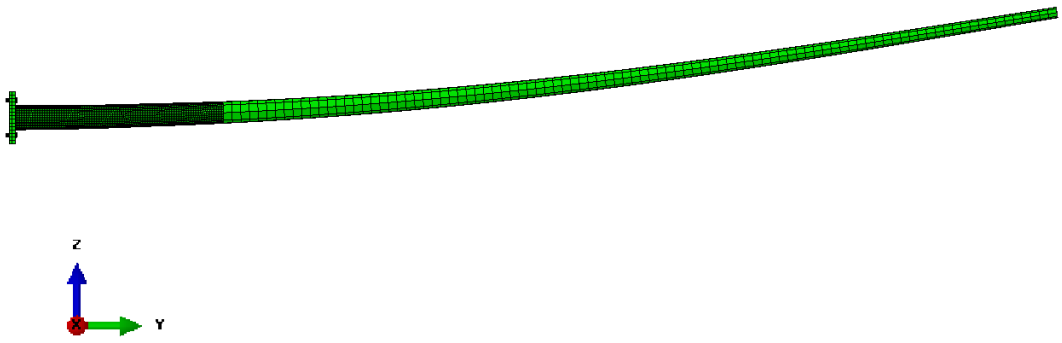

Figure 4-12: Second mode shape in Z-Y plane

the curvature differences between intact model and damaged models. The curvature difference is computed by Equation (4.20).

$$\Delta r_{\phi_n''} = \frac{\phi_n''|_{damaged}}{\phi_n''|_{intact}} \tag{4.20}$$

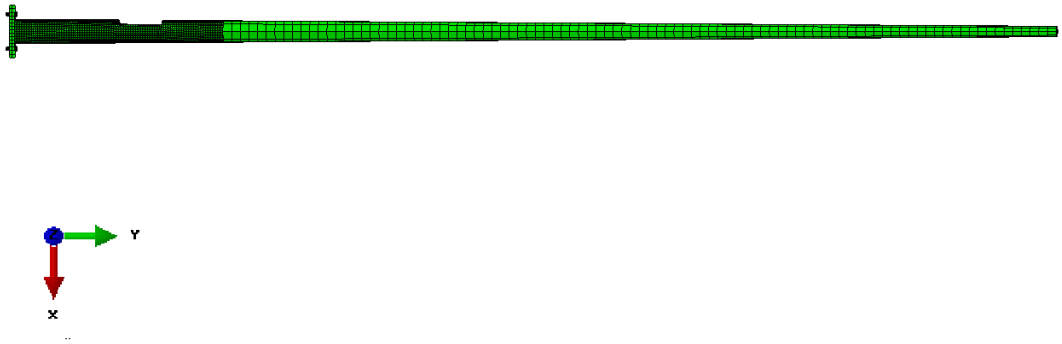

Figure 4-13: Second mode shape in X-Y plane

From those figures, one can tell that when the damage area exceed 80 %,(Figures (4-14)and(4-15) the peak value of curvature difference can directly used to identify the damage location; when damage area is between 40% to 60%, there were shift in peak values; when damage area is lower than 20%, which can be used to represent initial damage in structure, the curvature difference is not sensitive enough to localize the damage.

As a result, curvature of mode shapes can be used to localize damages, however, it is not sensitive to initial damage(damage area that smaller than 20 %)

4.5 Proposed methodology for damage identification in light poles

The damage detection methodology is presented in following,

1. Extract first 10 model frequencies/ mode shapes from an intact model and unknown models;

2. Compute the modal frequency differences and changes in mode shapes of the unknown light poles;

3. Compute thresholds t_s and t_i, and use them to determine sensitive/insensitive modes;

4. Locate the damage by checking the combination of sensitive and insensitive modes of unknown light poles in Table4.10 (Check Table 4.21 in blind-tests); or locate the damage by finding the location of maximum change in second mode shape curvature $r_{\phi'',max}$;

5. Use obtained linear/non-linear equations to quantify the damage.

The damage detection method using modal frequency are illustrated by the flow chart in Fig 4-19.

Fig 4-20 shows the procedure of damage detection using curvatures of mode shapes. Fig 4-21 shows the procedure of damage detection without an intact light pole.

4.6 Summary

In this chapter, three different damage cases of FE light pole model were reported at first. Their results are concluded into a damage detection method using modal frequency difference of light poles, including localization and quantification of the damage size and level.

- The combination of sensitive modes and insensitive modes can be used as indicators for locating damages. As shown in table 4.10, the combination of sensitive and insensitive modes is unique for each damage location. By finding the unique combination, one can locate a damage in light pole. For example, if the sensitive modes of an unknown light pole is 1^{st} mode and 7^{th} mode, and the insensitive mode is 6^{th} mode, it can be clam that a damage locates at L_1.

- For each damage location, two equations were determined for expressing the relationships among damage sizes, damage levels and modal frequency differences.

- A blind-test method using an arbitrary unknown light pole as baseline for identifying sensitive/insensitive modes was introduced for damage detection when intact model is unavailable. However, this method must be applied with an assumption: all damaged models have different damages with each other. With this assumption, the baseline light pole is always different from other light poles.

- Damage detection method using curvatures of second mode shape was also reported. The peak value of mode shape curvature change ($r_{\phi''}$) occurs at damage location.

- At last, a damage detection methodology was proposed to identify a damage in light poles.

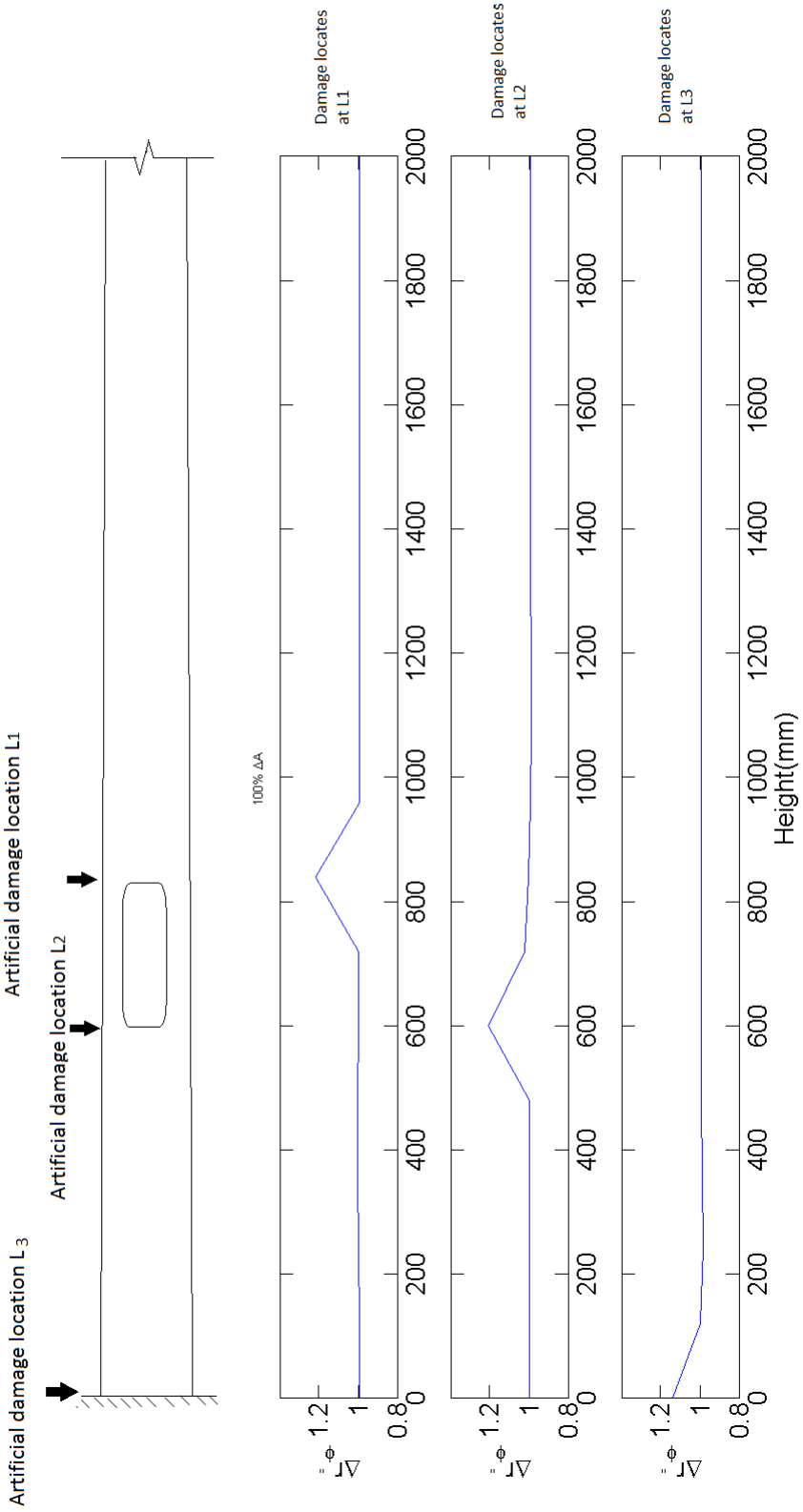

Figure 4-14: Changes in curvature of 100 %damage area scenario

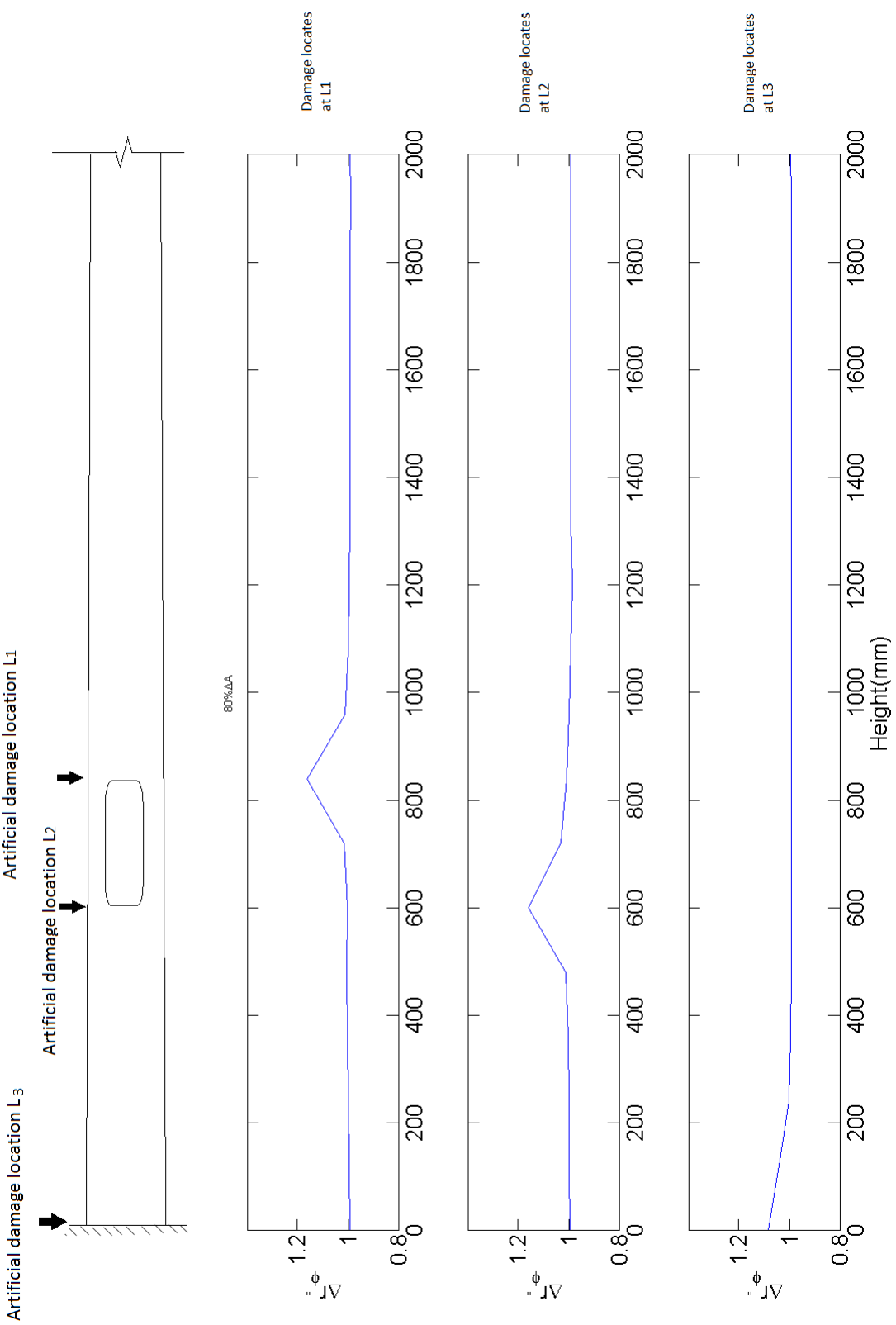

Figure 4-15: Changes in curvature of 80 %damage area scenario

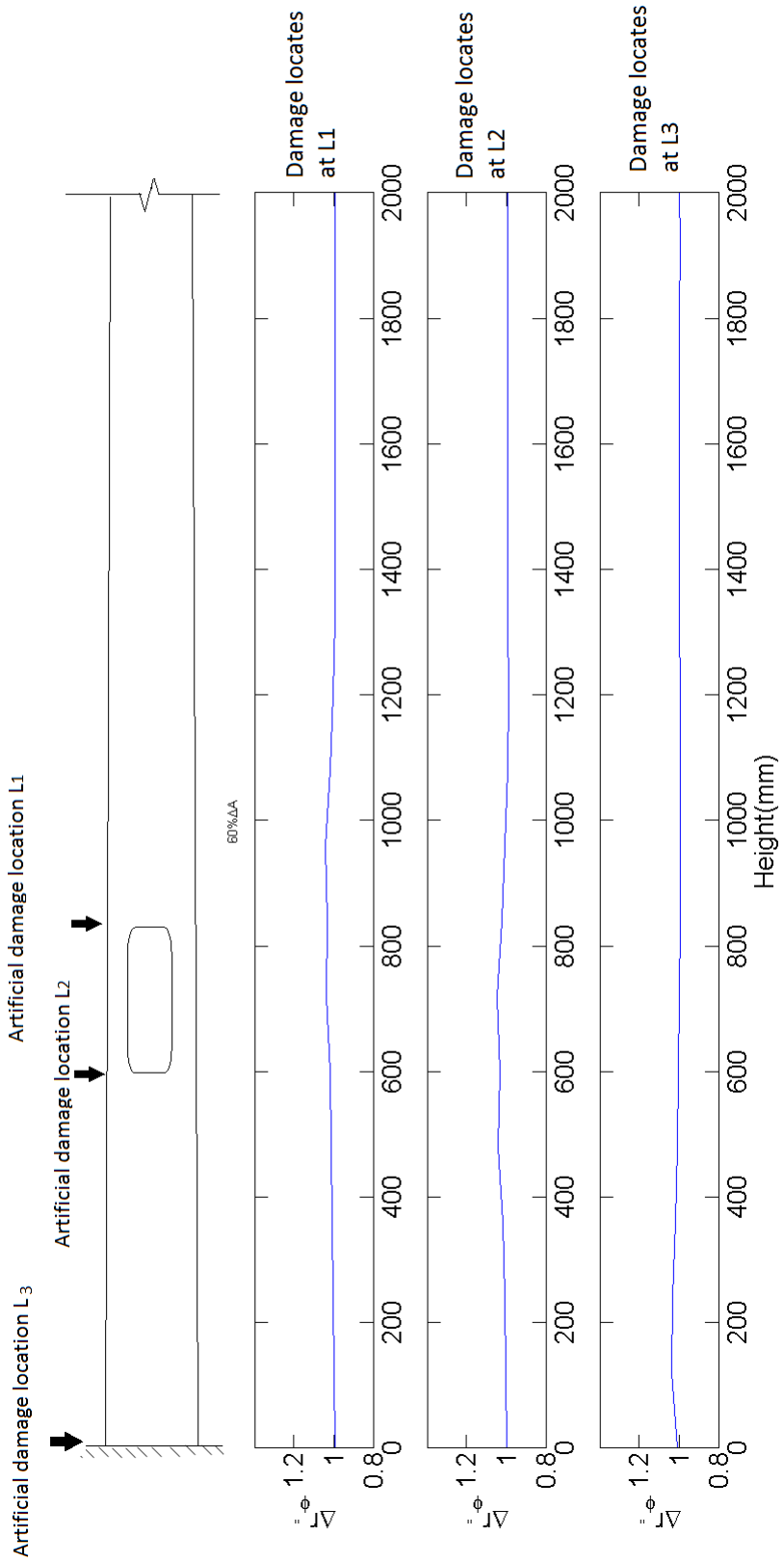

Figure 4-16: Changes in curvature of 60 %damage area scenario

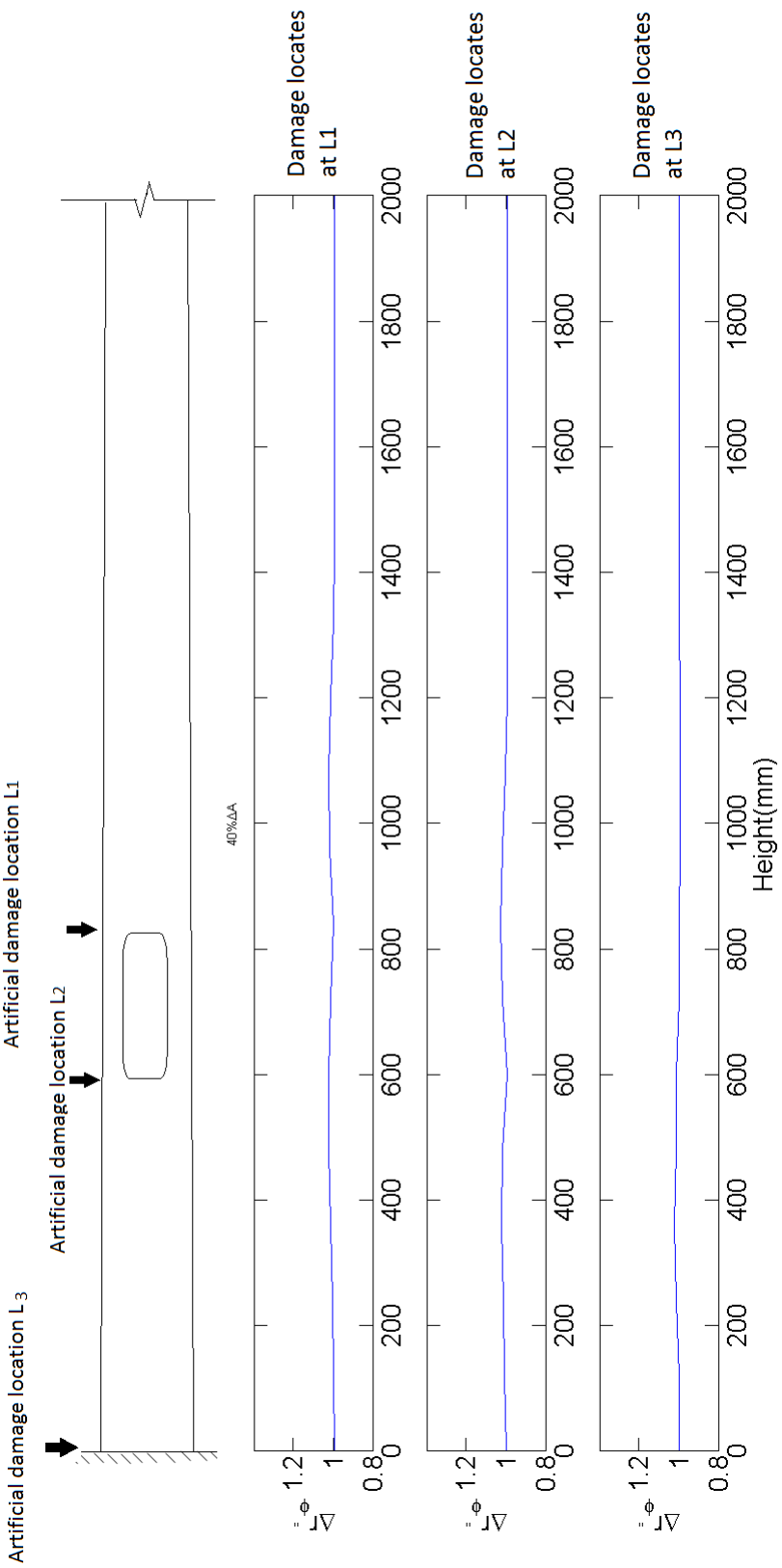

Figure 4-17: Changes in curvature of 40 %damage area scenario

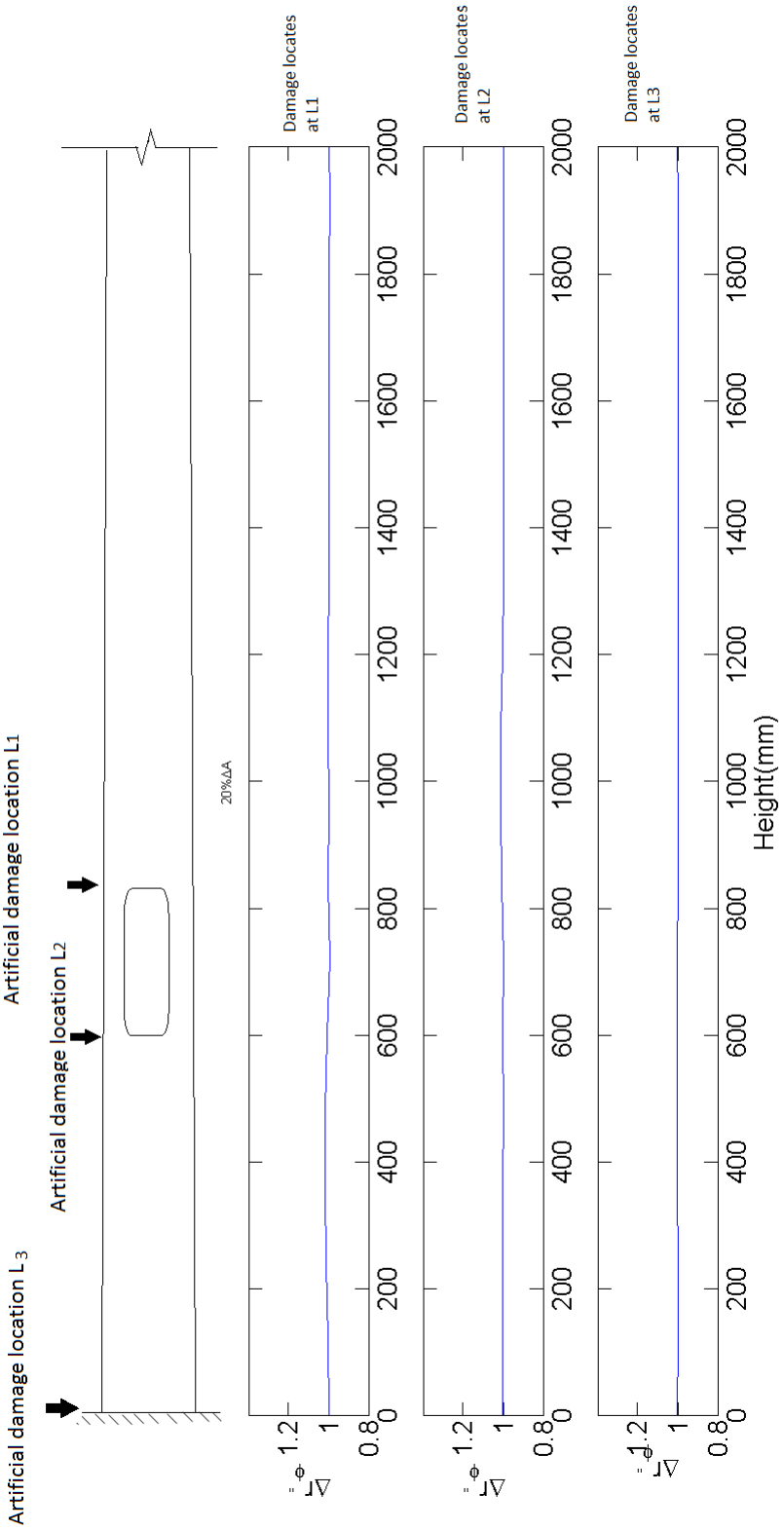

Figure 4-18: Changes in curvature of 20 %damage area scenario

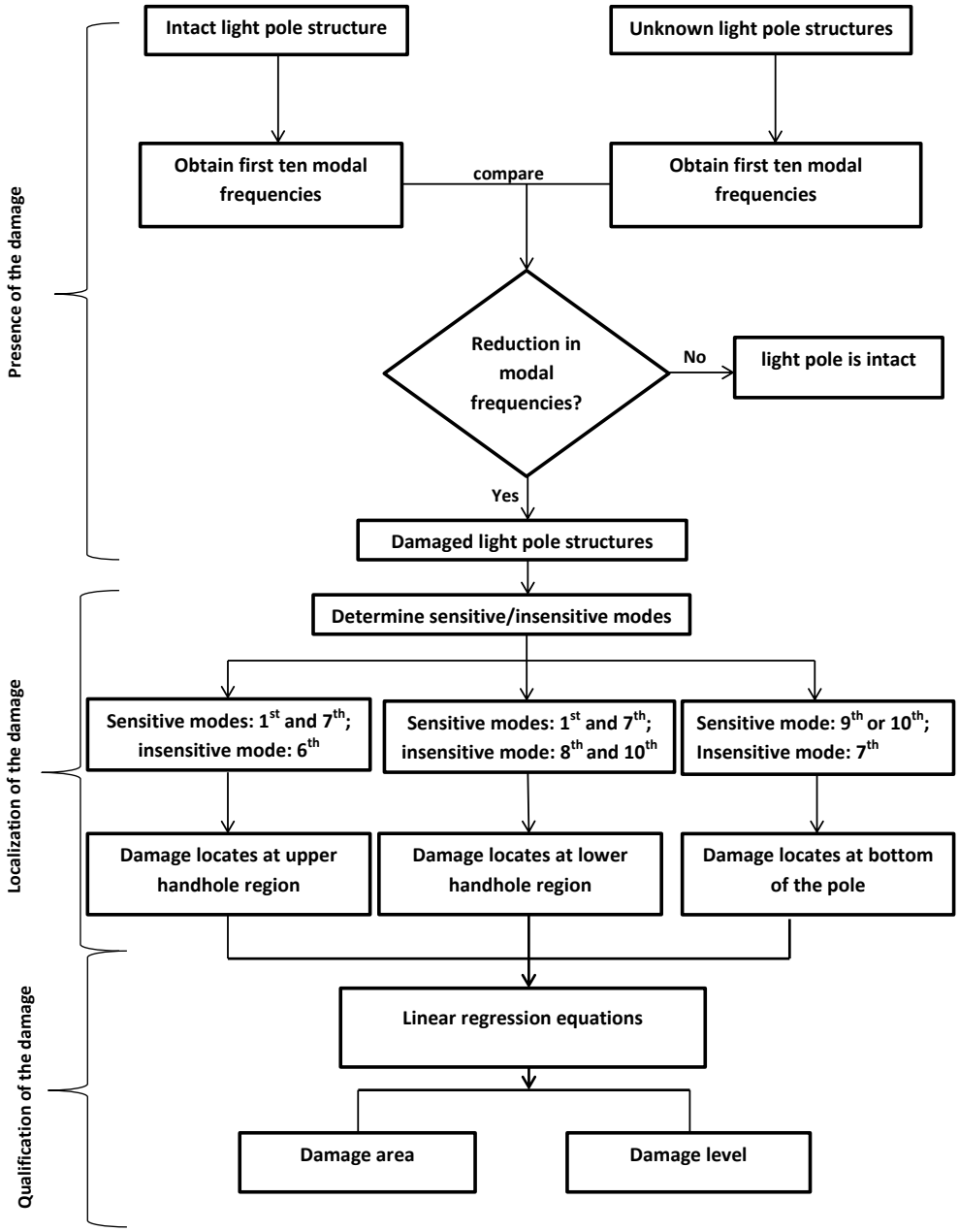

Figure 4-19: Damage detection methodology using modal frequencies with intact light pole

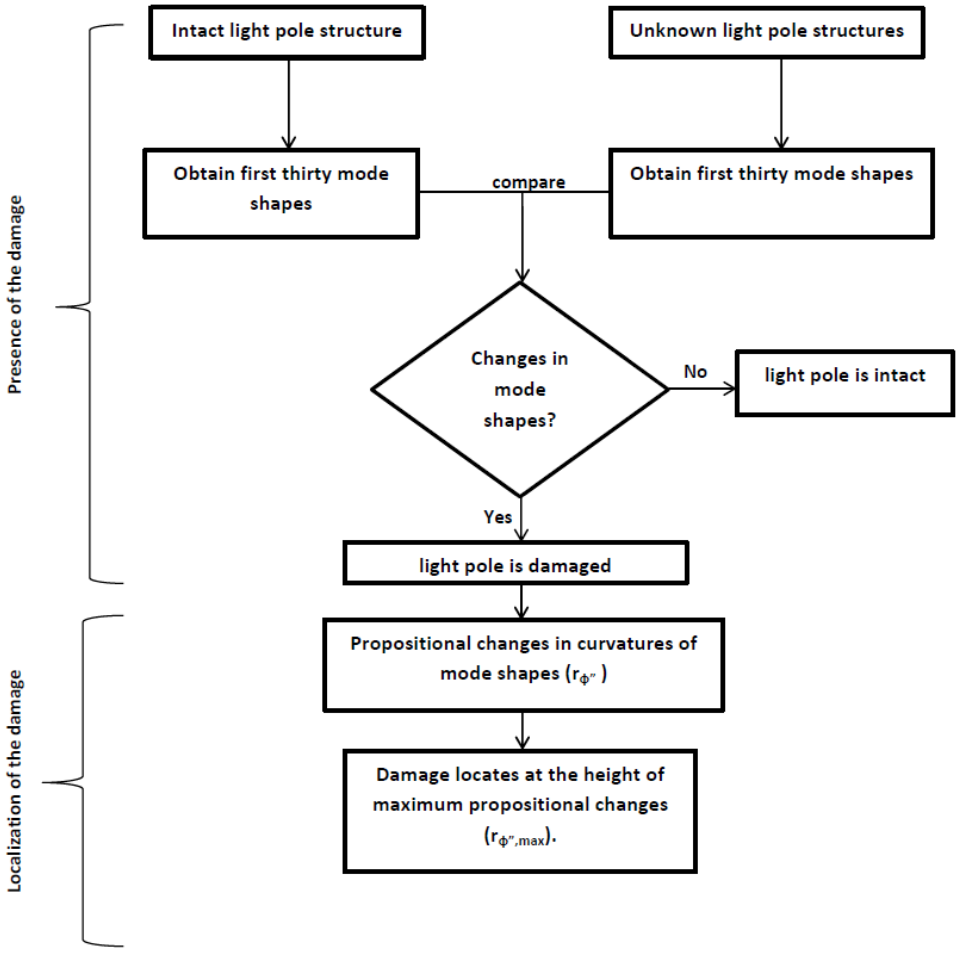

Figure 4-20: Damage detection procedures using mode shapes with intact light pole

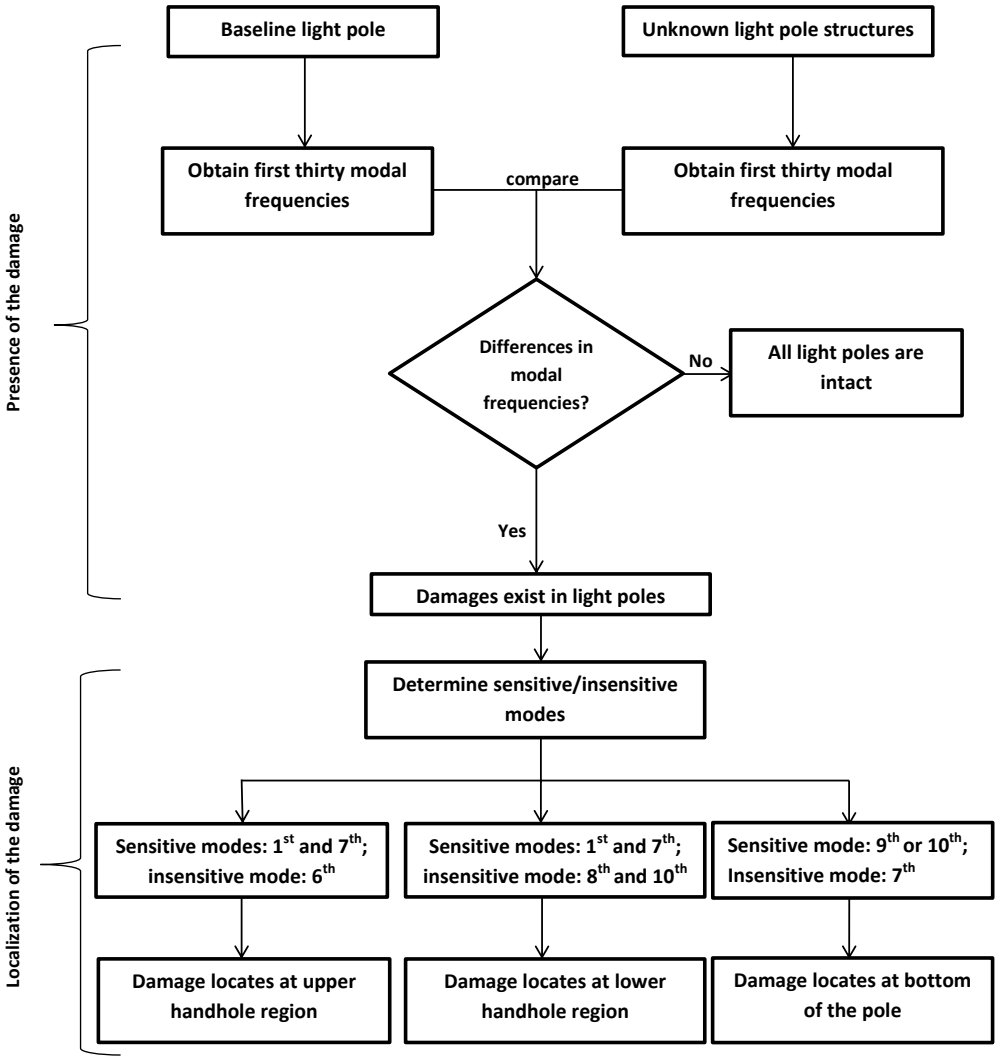

Figure 4-21: Damage detection procedures for blind-test

Chapter 5

Conclusion

In this chapter, research findings, contributions and the future work of this study are reported.

5.1 Research Findings

The research findings of this study are summarized:

- Damage location - The combination of sensitive modes and insensitive modes can be used as indicators for locating damages. The introduction of damage reduces light pole's structural stiffness, which results in decrease in light poles' modal frequencies (modal frequency difference, different from mode to mode). It is found that the combination of sensitive modes and insensitive modes is unique for each damage location. By checking the combination of sensitive modes and insensitive modes of an unknown light pole, one can locate the damage of light poles (for the case considered in this research). The combination of sensitive and

in sensitive modes for each damage location is shown in Table 4.10. For example, the combination of sensitive modes 1 and 7 with insensitive mode 6 suggests a possible damage characterized by 20% ~100% damage size and 10%~90% aging deterioration at location L_1 (upper region of a hand hole in a light pole). However, in practice, the identification of insensitive modes may be affected by noise. Alternatively, one can use sensitive modes to the locate damage.

- Damage size - When increasing damage size/level, light pole stiffness reduction also increases, which results in the increase of modal frequency difference. It means that, the greater modal frequency difference, the more severe the deterioration that may exist in light pole. Assuming the reduction in Young's modulus is constant as 50% (ΔE=50%), the relationship between damage size $\alpha^j A$ and modal frequency difference Δf_i^j can be described by Eq (5.1) for each damage location (tabulated in Table 5.1). This equation can be used for quantification of damage size. For example, a damaged light pole's Young's modulus of deteriorated region reduces 50%, and damage locates at upper region of the handhole (L_1). The 10th modal frequency difference is predicted as 0.5206% ($\Delta f_{10}^1 = 0.5206\%$). Substituting $\Delta f_{10}^1 = 0.5206\%$ into Eq (5.1) gives a result that $\alpha^1 = 0.4$. This result suggests that 40% area of upper handhole region is deteriorated.

- Damage level - When the damage size is constant as ($\Delta A = 100\%$), relationship between damage level $\beta^j E$ and modal frequency difference Δf_i^j is found and can be described by a logarithmic equation (Eq (5.2)) for each damage location (tab-

ulated in Table 5.2). For example, assume that i) entire cross-section is damaged ($\Delta A = 100\%$), ii) damage location the at upper region of the handhole (L_1). At the 10th mode, 0.5814% ($\Delta f_2^1 = 0.5206\%$) of modal frequency change is predicted. Substitute Δf_2^1 in Eq (5.2), then $\beta^1 = 0.5$, suggesting that the Young's modulus of damaged region is reduced by 50%. Table 5.1 shows the coefficients of Eq (5.1) for different damage sizes. Table 5.2 shows the coefficients of Eq (5.2) for different damage levels.

$$\alpha^j = a\Delta f_i^j + b \tag{5.1}$$

$$\beta^j = c\ln(\Delta f_i^j) + d \tag{5.2}$$

Table 5.1: Relationships between damage size $\alpha^j A$ and modal frequency difference Δf_i^j

Location(j)	Best-fit mode(i)	a	b	R^2
1	10	0.0255	0.4614	0.9841
2	6	0.0526	0.1665	0.9966
3	4	0.6858	-0.1251	0.9750

Table 5.2: Relationship between damage level $\beta^j E$ and modal frequency difference Δf_i^j

Location(j)	Best-fit mode(i)	c	d	R^2
1	2	-0.195	0.3900	0.9911
2	2	-0.194	0.3879	0.9914
3	8	-0.199	0.3628	0.9914

- Without an intact modal - In some cases, intact light pole is unknown (blind-test). One can use adjusted method to determine sensitive modes and insensitive modes for damage localization. Since light poles are installed by multiply, one can always collect a set of data (i.e., modal frequency) from light poles of similar designs in similar environments. Therefore, their damage conditions are similar.

Obtain modal frequency differences by selecting an arbitrary, unknown light pole as baseline (instead of an intact light pole) and then determine the sensitive and insensitive modes of the light poles under test. It is found that, in blind-test, the combination of sensitive and insensitive modes for each damage location are similar to the tests with an intact light pole. Therefore, by utilizing Table 4.10, damages can be located. This method can be applied as long as the baseline light pole is similar to other light poles under test and no damage light poles are identical.

- Mode shape curvature - As reported in Chapter 2, curvature of mode shapes are more sensitive to damage location than modal frequency. In the 2^{nd} mode, curvature changes the most at damage location. Inversely, one can use changes in the curvature of the 2^{nd} mode shape to localize damages. However, this method is limited. Only when the damage size is greater than 80% of cross-section area, the maximum curvature changes can accurately locate damages. When damage size is between 40% to 60% of cross-sectional area, there will be shifts between the maximum curvature change location and the damage location; when damage size is lower than 20% of cross-sectional area, the curvature change is not sensitive to localize the damage.

5.2 Contributions

Potential damages in a light pole can be identified and quantified by using the changes in modal frequencies and mode shapes. In this study, the relationships among those

changes and damages were investigated and used for damage identification.

- Sensitive modes and insensitive modes of light poles are defined, and their combinations are found to be unique for each damage location. In the other words, damage location can be determined by finding out the sensitive modes and insensitive modes of a light pole, and check for the corresponding damage location.

- Reliability of sensitive modes is validated by theoretical calculation.

- The relationships among damage attributes (damage locations, damage sizes and damage levels) and modal frequency difference are described by two equations. They can be used to qualify damages in light poles.

- A Damage detection methodology IS proposed to identify the damages in a light pole structure using its dynamic responses (modal frequencies and mode shapes) in free vibration.

5.3 Future work

While conclusions and damage detection methodology have developed from this study, there are a number of areas that deserve further attention. Physical experiments needs to be conducted in order to confirm the FE simulation results. A damage quantification method using changes in mode shape's curvature also needs additional works on it. Furthermore, since practically extracting first ten modal frequencies of a light pole is very difficult, a damage detection methodology using fewer modal frequencies(e.g.,

first four modal frequencies) needs to be developed in the future. In addition, the relationship between HSR (Appendix A) and damage attributes can studied. At last, more damage locations (*e.g.* the conjunctive weld between pole and base plate) can be explored.

Appendix A

The Effects of High Stress Region (HSR)

Due to various shapes of vibration modes, stresses are distributed differently from one mode to another. High stress region (HSR) are defined as: in one vibration mode, those regions which have stresses higher than 50 % of maximum stress in the entire model. (i.e., $\sigma > \sigma_{max}$.)

Figure A-1 shows the cross-sectional stress distribution of intact model at mode 12, at location L_3. The maximum stress of the model is 41.94 Mpa, and 50% of maximum stress in model is 50%*41.94=20.97 Mpa. In this cross-section, cells with warmest color in Figure A-1 have stress of 33.0393 MPa, while the cells with coolest color have 5.5321 MPa. Those cells in which have stress higher than 20.97 formed a high stress region(HSR).

It was observed that appearance of high stress region in the artificially damage area, leads to significant reduction in modal frequencies comparing with artificial damage

without high stress region. For example, Figure A-4 is modal frequency differences of five damaged models with five different damage areas (damages were located at location L_3 and Young's modulus reduced by 50 %). Notice that, in the cross-sectional plane in Figure A-1, high stress regions appear between edges of 40 % and 60%. In Figure A-4, in mode 12, reduction in modal frequency has a notable "jump" while enlarging damaged area from 40% to 60%. Similar "jump" occurs in mode 13 (Figure A-2), while increasing the damaged region' area from 80% to 100%, wherein high stress region appear. However, from edges 0% to 80% of damaged region's area no high stress region was appear inside damaged region. Meanwhile, no "jump" is observed. It was also observed that when there is no high stress region exists in damage region, such as mode 7(Figure A-3), modal frequencies' reduction changes slightly. (This phenomenon ('jump') is observed in any vibration mode of any damage location as long as there is a high stress region.)

In Chapter 4, sensitive modes are defined as the modes in which their modal frequency differences are higher than 1.25 times average modal frequency difference. Since the appearance of HSR in artificial damage area would cause significant reduction in modal frequencies, it could be the explanation for sensitive modes. For example, the sensitive modes for damage locates at L_3 are 12th and 15th vibration modes. Compare the cross-sectional stress distribution of 12th mode (sensitive mode) and 7th mode, it can be observed: 12th mode (HSR is appear in artificially damaged region) has larger modal frequency difference than 7th mode (no HSR is appear in artificially damaged region). Also, compare the cross-sectional stress distribution of 12th mode (sensitive mode) and 13th mode, it can be observed: 12th mode has larger modal frequency difference than

13th mode (cross-section of 12th mode contains larger HSR area than 13 mode).

From above observations, three conclusions were made: 1) superposition of damage region and HSR lead to larger modal frequency difference, 2) the more HSRs are contained in damaged region, the larger modal frequency difference are caused and hence 3) those modes with larger modal frequency differences (larger than thresholds) can be defined as sensitive modes, which indicate HSR's contribution to sensitive modes.

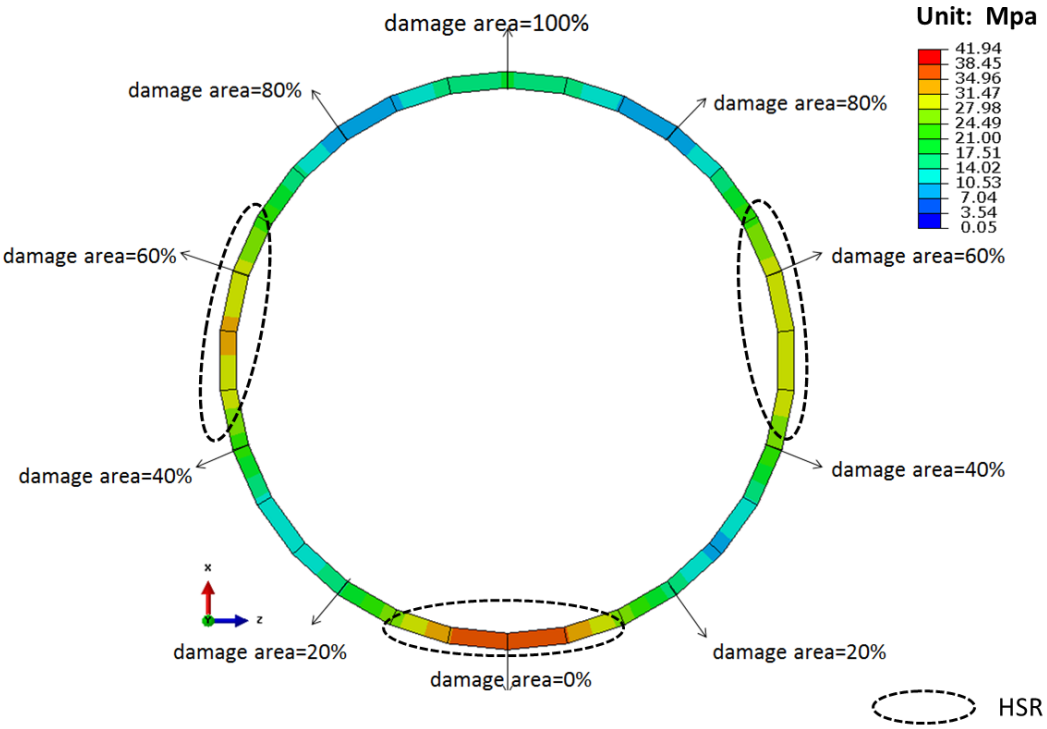

Figure A-1: Mode 12–Cross sectional stress distribution locate at L_3

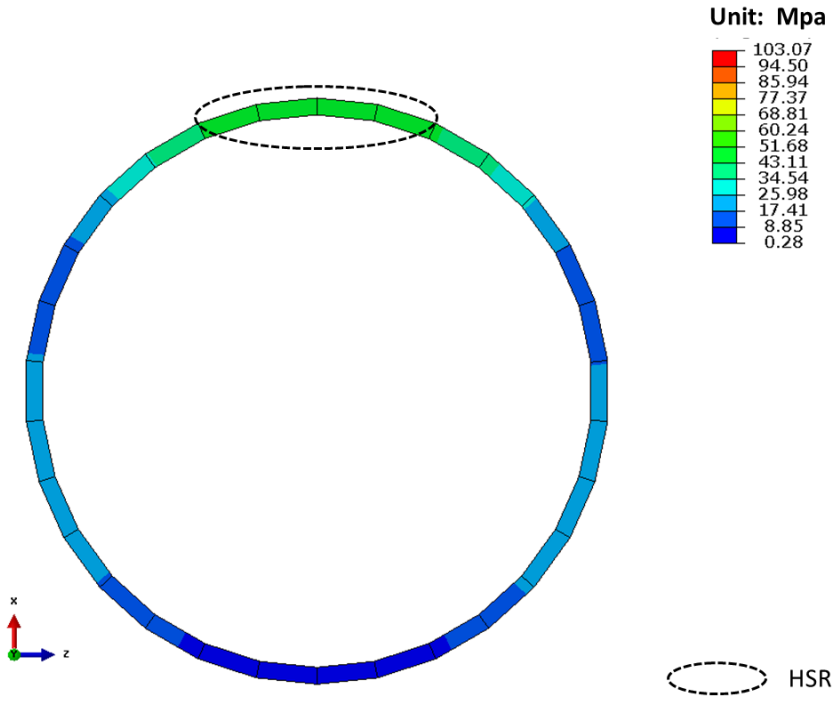

Figure A-2: Mode 13–Cross sectional stress distribution locate at L_3

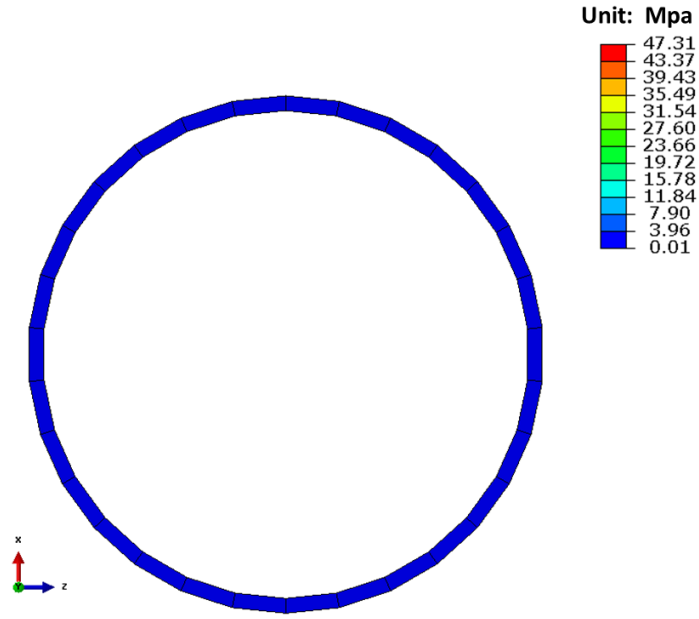

Figure A-3: Mode 7–Cross sectional stress distribution locate at L_3

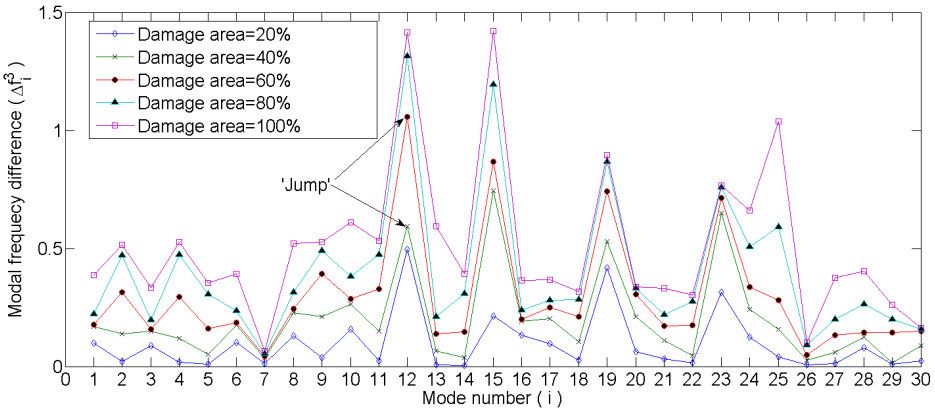

Figure A-4: Modal frequency differences of different damages at location *L*3

Appendix B

Modal Frequencies of FE models

Table B.1: L_1, E=50%, with varying damage sizes α (Hz)

	INTACT	α=20%	α=40%	α=60%	α=80%	α=100%
Mode 1	3.42131	3.39177	3.3872	3.38634	3.38277	3.37601
Mode 2	3.99898	3.98932	3.98296	3.97867	3.97626	3.97573
Mode 3	16.9102	16.8865	16.8804	16.8796	16.8757	16.8678
Mode 4	17.4531	17.4003	17.3958	17.3922	17.3881	17.3867
Mode 5	41.2469	41.0224	40.9747	40.9595	40.9564	40.9543
Mode 6	44.3003	44.2948	44.2897	44.288	44.2872	44.2857
Mode 7	68.3359	67.6588	67.3888	67.2838	67.2689	67.2658
Mode 8	83.8118	83.6539	83.6391	83.6291	83.6226	83.616
Mode 9	96.2322	95.7698	95.6759	95.639	95.624	95.6117
Mode 10	132.922	132.282	132.23	132.207	132.177	132.139

Table B.2: L_2, E=50%, with varying damage sizes α (Hz)

	INTACT	α=20%	α=40%	α=60%	α=80%	α=100%
Mode 1	3.42131	3.39277	3.38927	3.38846	3.38494	3.37796
Mode 2	3.99898	3.99326	3.98472	3.97914	3.97664	3.97615
Mode 3	16.9102	16.8493	16.8441	16.8422	16.8364	16.8258
Mode 4	17.4531	17.4337	17.4012	17.3833	17.3781	17.3771
Mode 5	41.2469	41.0446	40.9837	40.9589	40.955	40.9532
Mode 6	44.3003	44.2219	44.2168	44.2129	44.2084	44.2028
Mode 7	68.3359	67.4053	67.3264	67.2943	67.2736	67.2651
Mode 8	83.8118	83.749	83.7357	83.7272	83.7252	83.7248
Mode 9	96.2322	95.7047	95.6676	95.6435	95.6214	95.6057
Mode 10	132.922	132.893	132.849	132.834	132.827	132.812

Table B.3: L_3, E=50%, with varying damage sizes α (Hz)

	INTACT	α=20%	α=40%	α=60%	α=80%	α=100%
Mode 1	3.42131	3.41789	3.41551	3.41521	3.41367	3.40811
Mode 2	3.99898	3.9981	3.9935	3.9864	3.98014	3.97842
Mode 3	16.9102	16.8954	16.885	16.8837	16.8769	16.8537
Mode 4	17.4531	17.4498	17.4326	17.4016	17.3704	17.3612
Mode 5	41.2469	41.2428	41.2253	41.1804	41.1211	41.1014
Mode 6	44.3003	44.2551	44.2226	44.2176	44.196	44.126
Mode 7	68.3359	68.3274	68.3116	68.3069	68.298	68.2917
Mode 8	83.8118	83.7023	83.6211	83.6064	83.5493	83.3763
Mode 9	96.2322	96.1958	96.0304	95.8547	95.7604	95.7249
Mode 10	132.922	132.713	132.571	132.543	132.417	132.11

Table B.4: L_1, α=50%, with varying damage levels E (Hz)

	INTACT	β=90%	β=70%	β=50%	β=30%	β=10%
Mode 1	3.42131	3.41586	3.40097	3.37601	3.3233	3.11191
Mode 2	3.99898	3.99633	3.98886	3.97573	3.94624	3.81305
Mode 3	16.9102	16.9051	16.8911	16.8678	16.8187	16.6286
Mode 4	17.4531	17.4449	17.4227	17.3867	17.3146	17.0595
Mode 5	41.2469	41.208	41.1075	40.9543	40.6783	39.9065
Mode 6	44.3003	44.2983	44.2934	44.2857	44.2712	44.2214
Mode 7	68.3359	68.19	67.8182	67.2658	66.3076	63.8065
Mode 8	83.8118	83.787	83.7212	83.616	83.4098	82.703
Mode 9	96.2322	96.144	95.9244	95.6117	95.1031	93.9135
Mode 10	132.922	132.824	132.561	132.139	131.304	128.472

Table B.5: L_2, α=50%, with varying damage levels E (Hz)

	INTACT	β=90%	β=70%	β=50%	β=30%	β=10%
Mode 1	3.42131	3.41611	3.40189	3.37796	3.32699	3.11893
Mode 2	3.99898	3.99639	3.98907	3.97615	3.94693	3.81244
Mode 3	16.9102	16.8998	16.8719	16.8258	16.7316	16.3877
Mode 4	17.4531	17.4438	17.4187	17.3771	17.2907	16.9572
Mode 5	41.2469	41.2084	41.1081	40.9532	40.6669	39.8316
Mode 6	44.3003	44.2879	44.2551	44.2028	44.1004	43.7612
Mode 7	68.3359	68.1924	67.8232	67.2651	66.2713	63.5936
Mode 8	83.8118	83.8003	83.7706	83.7248	83.6395	83.3774
Mode 9	96.2322	96.1455	95.9265	95.6057	95.0604	93.6937
Mode 10	132.922	132.908	132.872	132.812	132.69	132.197

Table B.6: L_3, α=50%, with varying damage levels E (Hz)

	INTACT	β=90%	β=70%	β=50%	β=30%	β=10%
Mode 1	3.42131	3.41982	3.41559	3.40811	3.39104	3.31124
Mode 2	3.99898	3.99665	3.99007	3.97842	3.95195	3.82951
Mode 3	16.9102	16.9038	16.8857	16.8537	16.7817	16.4582
Mode 4	17.4531	17.4426	17.413	17.3612	17.2457	16.7478
Mode 5	41.2469	41.23	41.183	41.1014	40.9232	40.2043
Mode 6	44.3003	44.2804	44.2244	44.126	43.9057	42.9451
Mode 7	68.3359	68.3306	68.3161	68.2917	68.2412	68.0589
Mode 8	83.8118	83.7618	83.6215	83.3763	82.8338	80.5797
Mode 9	96.2322	96.1739	96.0103	95.7249	95.0948	92.4905
Mode 10	132.922	132.828	132.565	132.11	131.126	127.364

Bibliography

[1] V. A. Pino, "Fatigue life prediction of cantilevered light pole structures," 2010.

[2] B. R. Reese, "Non-destructive examination techniques of tubular steel pole sports lighting structures.".

[3] J. Shortsleeve, "I-team: Aging light poles a safety concern on Mass. roads." `http://boston.cbslocal.com/2012/10/31/`, 2012.

[4] R.J.Connor, J.Ocel, and B.Brakke, "Fatigue cracking and inspection of high-mast lighting towers," Tech. Rep. IBC-05-31, Iowa and Pennsylvania Departments of Transportation, Pennsylvania Infrastructure Technology Alliance (PITA), 2005.

[5] M. J. Garlich and E. T. Thorkildsen., "Guidelines for the installation, inspection, maintenance and repair of structural supports for highway signs, luminaires, and traffic signals," Tech. Rep. FHWA NHI 05-036, Office of Bridge Technology Federal Highway Administration, 2005.

[6] M. R. K. et al, "NCHRP report 412: Fatigue-resistant design of cantilevered signal, sign and light supports," Tech. Rep. HR 10-38, ATLSS Engineering Research Center, 1998.

[7] L. Caracoglia and N. P. Jones, "Analysis of light pole failures in illinois - final report," Tech. Rep. UILU-ENG-2004-2007, Department of Civil and Environmental Engineering University of Illinois at Urbana-Champaign, 2004.

[8] Y. J. Yan, L. H. Yam, L. Cheng, and L. Yu, "Fem modeling method of damage structures for structural damage detection," *Composite Structures*, vol. 72, pp. 193–199, 2006.

[9] T. Lea, A. Abolmaalia, S. A. Motaharia, W. Yeihb, and R. Fernandezc, "Finite element-based analyses of natural frequencies of long tapered hollow steel poles," *Journal of Constructional Steel Research*, vol. 64, pp. 275–284, 2008.

[10] Dassault Systémes, 10 rue Marcel Dassault, CS 40501, 78946 Vélizy-Villacoublay Cedex - France, *Abaqus/CAE User's Manual Version 6.11, http://abaqus.ethz.ch:2080/v6.11/.*

[11] L. H. Yam, Y. J. Yan, and Z. Wei, "Vibration-based non-destructive structural damage detection, advances in nondestructive evaluation," *Key Engineering Materials*, vol. 270-273, pp. 1446–1453, 2004.

[12] Y. J. Yan, Z. Y. W. L. Cheng, and L. H. Yam, "Development in vibration-based structural damage detection technique," *Mechanical Systems and Signal Processing*, vol. 21, pp. 2198–2211, 2007.

[13] M. K. Yoon, D. Heider, J. W. Gillespie, C. P. Ratcliffe, and R. M. Crane, "Local damage detection using the two-dimensional gapped smoothing method," *Journal of Sound and Vibration*, vol. 279, pp. 2198–2211, 2005.

[14] H. V. der Auweraer, "International research projects on structural damage detection," *Damage Assessment of Structures Key Engineering Materials*, vol. 204-2, pp. 97–112, 2001.

[15] E. P. Carden and P. Fanning, "Vibration based condition monitoring: A review," *Structural Health Monitoring*, vol. 3 (4), pp. 355–377, 2004.

[16] R. P. C. Sampaio, N. M. M. Maia, and J. M. M. Silva, "The frequency domain assurance criterion as a tool for damage detection," *Proceedings Key Engineering Materials*, vol. 245-2, pp. 69–76, 2003.

[17] Z. Y. Shi, S. S. Law, and L. M. Zhang, "Structural damage detection from modal strain energy change," *Journal of Engineering Mechanics- ASCE*, vol. 126 (12), pp. 1216–1223, 2000.

[18] J. T. Kim, Y. S. Ryu, H. M. Cho, and N. Stubbs, "Damage identification in beam-type structures: frequency-based method vs. mode-shapebased method," *Engineering Structures*, vol. 25 (1), pp. 57–67, 2003.

[19] Y. S. Lee and M. J. Chung, "A study on crack detection using eigenfrequency test data," *Computers Structures*, vol. 77 (3), pp. 327–342, 2000.

[20] H. Z. Yang, H. J. Li, and S. Q. Wang, "Damage localization of offshore platforms under ambient excitation," *China Ocean Engineering*, vol. 17 (4), pp. 495–504, 2003.

[21] L. M. Khoo, P. R. Mantena, and P. Jadhav, "Structural damage assessment using vibration modal analysis," *Structural Health Monitoring*, vol. 3 (2), pp. 177–194, 2004.

[22] Y. Aoki and O. I. Byon, "Damage detection of cfrp pipes and shells by using localized flexibility method," *Advanced Composite Materials*, vol. 10 (2-3), pp. 189–198, 2001.

[23] A. M. Yan and J. C. Golinval, "Structural damage localization by combining flexibility and stiffness methods," *Engineering Structures*, vol. 27 (12), pp. 1752–1761, 2005.

[24] N. G. Park and Y. S. Park, "Identification of damage on a substructure with measured frequency response functions," *Journal of Mechanical Science and Technology*, vol. 19 (10), pp. 1891–1901, 2005.

[25] A. Furukawa, H. Otsuka, and J. Kiyono, "Structural damage detection method using uncertain frequency response functions," *Computer- Aided Civil And Infrastructure Engineering*, vol. 21 (4), pp. 292–305, 2006.

[26] A. Iwasaki, A. Todoroki, Y. Shimamura, and H. Kobayashi, "Unsupervised structural damage diagnosis based on change of response surface using statistical tool (application to damage detection of composite structure)," *SME International Journal Series A-Solid Mechanics and Material Engineering*, vol. 47 (1), pp. 1–7, 2004.

[27] M. L. Fugate, H. Sohn, and C. R. Farrar, "Vibration-based damage detection using statistical process control," *Mechanical Systems and Signal Processing*, vol. 15 (4), pp. 707–721, 2001.

[28] J. Lopez-Diez, M. Torrealba, A. Guemes, and C. Cuerno, "Application of statistical energy analysis for damage detection in spacecraft structures," *Damage Assessment of Structures Vi Key Engineering Materials*, vol. 525-532, p. 1?7, 2005.

[29] T. Y. Li, T. Zhang, J. X. Liu, and W. H. Zhang, "Vibrational wave analysis of infinite damaged beams using structure-borne power flow," *Applied Acoustics*, vol. 65 (1), pp. 91–100, 2004.

[30] D. Mahapatra and S. Gopalakrishnan, "Spectral finite element analysis of coupled wave propagation in composite beams with multiple delaminations and strip inclusions," *International Journal of Solids and Structures 41*, vol. 5-6, pp. 1173–1208, 2004.

[31] S. Rajasekaran and S. P. Varghese, "Damage detection in beams and plates using wavelet transforms," *Computers and Concrete*, vol. 2 (6), pp. 481–498, 2005.

[32] C. J. Lu and Y. T. Hsu, "Vibration analysis of an inhomogeneous string for damage detection by wavelet transform," *International Journal of Mechanical Sciences*, vol. 44 (4), pp. 745–754, 2002.

[33] S. S. Law, X. Y. Li, X. Q. Zhu, and S. L. Chan, "Structural damage detection from wavelet packet sensitivity," *Engineering Structures*, vol. 27 (9), pp. 1339–1348, 2005.

[34] Y. J. Yan and L. H. Yam, "Online detection of crack damage in composite plates using embedded piezoelectric actuators/sensors and wavelet analysis," *Composite Structures*, vol. 58 (1), pp. 29–38, 2002.

[35] K. Moslem and R. Nafaspour, "Structural damage detection by genetic algorithms," *AIAA Journal*, vol. 40 (7), pp. 1395–1401, 2002.

[36] J. H. Chou and J. Ghaboussi, "Genetic algorithm in structural damage detection," *Computers Structures*, vol. 79 (14), pp. 1335–1353, 2001.

[37] Z. Y. Shi, S. S. Law, and L. Zhang, "Structural damage detection form modal strain energy change," *Journal of Engineering Mechanics ASCE*, vol. 26, pp. 1216–1223, 2000.

[38] C. Y. Kao and S. L. Hung, "Detection of structural damage via free vibration responses generated by approximating artificial neural networks," *Computers Structures*, vol. 81 (28-29), pp. 2631–2644, 2003.

[39] Q. Chen and K. W. Y. W. Chan, "Structural fault diagnosis and isolation using neural networks based on response-only data," *Computers Structures*, vol. 81 (22-23), pp. 2165–2172, 2003.

[40] K. Yuen and H. Lam, "On the complexity of artificial neural networks for smart structures monitoring," *Engineering Structures*, vol. 28, pp. 977–984, 2006.

[41] Y. Lee and M. Chung, "A study on crack detection using eigenfrequency test data," *Computers and Structures*, vol. 64, pp. 327–342, 2000.

[42] P. Gudmundson, "Eigenfrequency changes of strutures due to cracks, notches or other geometrical changes," *Journal of Mechanics and Physics of Solids*, vol. 30, pp. 339–53, 1982.

[43] D. Armon, Y. Ben-Haim, and S. Braun, "Crack detection in beams by rank-ordering of eigenfrequency shift," *Mechanical Systems and Signal Processing*, vol. 8, pp. 81–91, 1994.

[44] J.-T. Kim and N. Stubbs, "Crack detection in beam-type structures using frequency data," *Journal of Sound and Vibration*, vol. 259 (1), pp. 145–160, 2003.

[45] G. M. Owolabi, A. S. J. Swamidas, and R. Seshadri, "Crack detection in beams using changes in frequencies and amplitudes of frequency response functions," *Journal of Sound and Vibration*, vol. 265, pp. 1–22, 2003.

[46] M. A. B. Abdo and M. Hori, "A numerical study of structural damage detection using changes in the rotation of mode shapes," *Journal of Sound and Vibration*, vol. 251 (2), pp. 227–239, 2002.

[47] J. T. Kim, H. M. C. Y. S. Ryu, and N. Stubbs, "Damage identification in beam-type structures: frequency-based method vs mode-shape-based method," *Engineering Structures*, vol. 25, pp. 57–67, 2003.

[48] J. He and Z. F. Fu, *Modal Analysis*. Butterworth Heiemann, 2001.

[49] A. K. Chopra, *Dynamics of structures*. third edition ed., 2007.